ORIGINAL RESEARCH

Interferon Regulatory Factor 7 Protects Against Vascular Smooth Muscle Cell Proliferation and Neointima Formation

Ling Huang, MS;* Shu-Min Zhang, MD;* Peng Zhang, PhD;* Xiao-Jing Zhang, PhD; Li-Hua Zhu, MD; Ke Chen, PhD; Lu Gao, MD; Yan Zhang, MD; Xiang-Jie Kong, BS; Song Tian, BS; Xiao-Dong Zhang, PhD; Hongliang Li, MD, PhD

***Background*—**Interferon regulatory factor 7 (IRF7), a member of the interferon regulatory factor family, plays important roles in innate immunity and immune cell differentiation. However, the role of IRF7 in neointima formation is currently unknown.

***Methods and Results*—**Significant decreases in IRF7 expression were observed in vascular smooth muscle cells (VSMCs) following carotid artery injury in vivo and platelet-derived growth factor-BB (PDGF-BB) stimulation in vitro. Compared with non-transgenic (NTG) controls, SMC-specific IRF7 transgenic (IRF7-TG) mice displayed reduced neointima formation and VSMC proliferation in response to carotid injury, whereas a global knockout of IRF7 (IRF7-KO) resulted in the opposite effect. Notably, a novel IRF7-KO rat strain was successfully generated and used to further confirm the effects of IRF7 deletion on the acceleration of intimal hyperplasia based on a balloon injury-induced vascular lesion model. Mechanistically, IRF7's inhibition of carotid thickening and the expression of VSMC proliferation markers was dependent on the interaction of IRF7 with activating transcription factor 3 (ATF3) and its downstream target, proliferating cell nuclear antigen (PCNA). The evidence that IRF7/ATF3-double-TG (DTG) and IRF7/ATF3-double-KO (DKO) mice abolished the regulatory effects exhibited by the IRF7-TG and IRF7-KO mice, respectively, validated the underlying molecular events of IRF7-ATF3 interaction.

***Conclusions*—**These findings demonstrated that IRF7 modulated VSMC proliferation and neointima formation by interacting with ATF3, thereby inhibiting the ATF3-mediated induction of PCNA transcription. The results of this study indicate that IRF7 is a novel modulator of neointima formation and VSMC proliferation and may represent a promising target for vascular disease therapy. **(*J Am Heart Assoc*. 2014;3:e001309 doi: 10.1161/JAHA.114.001309)**

Key Words: ATF3 • IRF7 • neointima formation • proliferation

Neointima formation, which is defined as a thickening of the intimal layer, is an important process involved in various diseases and their treatments, eg, atherosclerosis, angioplasty, in-stent restenosis, vein bypass graft failure, transplant vasculopathy, and surgical repair.[1,2] This pathological condition reflects the complex cross-talk between vascular smooth muscle cells (VSMCs) and several cell types, including endothelial cells, inflammatory cells, and immune cells, resulting in the induction of VSMC phenotype switching and proliferation, a process that is critically involved in neointima formation and development.[3] In normal adult blood vessels, VSMCs exhibit quiescence and a low rate of proliferation.[4] However, after vascular endothelial injury, platelets, leukocytes, and SMCs are activated to release growth factors, such as platelet-derived growth factor (PDGF), to subsequently stimulate the alteration of VSMCs to a synthetic state.[5] Synthetic VSMCs are susceptible to undergoing proliferation, which is accompanied by the elevated expression of proliferation markers, such as proliferating cell nuclear antigen (PCNA) and Cyclin D1. However, the underlying molecular events involved in vascular injury-associated VSMC proliferation remain elusive. Therefore, the identification of regulatory factors would facilitate the development of therapies to counterbalance VSMC proliferation and to further

From the Department of Cardiology, Renmin Hospital of Wuhan University, Wuhan, China (L.H., S.-M.Z., P.Z., L.-H.Z., Y.Z., X.-J.K., S.T., H.L.); Cardiovascular Research, Institute of Wuhan University, Wuhan, China (L.H., S.-M.Z., P.Z., L.-H.Z., Y.Z., X.-J.K., S.T., H.L.); State Key Laboratory of Quality Research in Chinese Medicine, Institute of Chinese Medical Sciences, University of Macau, Macao, China (X.-J.Z.); College of life sciences, Wuhan University, Wuhan, China (K.C., X.-D.Z.); Department of Cardiology, Institute of Cardiovascular Disease, Union Hospital, Tongji Medical College, Huazhong University of Science and Technology, Wuhan, China (L.G.).

*Dr Huang, Dr Shu-Min Zhang, and Dr Peng Zhang contributed equally to the work.

Correspondence to: Hongliang Li, MD, PhD, Department of Cardiology, Renmin Hospital of Wuhan University, Cardiovascular Research Institute, Wuhan University, Jiefang Road 238, Wuhan 430060, China. E-mail: lihl@whu.edu.cn

Received August 13, 2014; accepted September 15, 2014.

ameliorate or prevent neointima formation and the resulting vascular diseases.

The interferon regulatory factor (IRF) family, which contains 9 members (IRF1−9) that share an amino-terminal 115-amino acid homology, plays important roles in innate immunity and immune cell differentiation through the transcriptional regulation of interferon (IFN)-induced signaling pathways.[6] Our previous studies demonstrated multiple functions of IRF members in various diseases, such as pathological cardiac hypertrophy,[7] ischemic stroke,[8] hepatic steatosis,[9] metabolic disorders,[10] and vascular diseases.[11] IRF7 is constitutively expressed in the cytoplasm of B cells, pDCs, and monocytes in the spleen and thymus and in peripheral blood lymphocytes. IRF7 is essential for inducing the expression of the type I *IFN* gene,[6,12] the negative regulator of arterial intimal lesions in vivo and in vitro,[13,14] which suggests that IRF7 potentially affects neointima formation. More recently, independent of IFN-regulated signaling pathways, IRF7 has been shown to be involved in cardiac hypertrophy,[15] obesity, insulin resistance,[16] stroke,[17,18] and endothelial cell infection-induced vascular lesions.[19] However, the precise function of IRF7 in VSMCs and neointima formation-induced vascular diseases is poorly understood.

In this study, we demonstrate that IRF7 inhibits neointima formation and VSMC proliferation in response to wire injury in mice and balloon injury in rats. Mechanistically, activating transcription factor 3 (ATF3) is identified as a pivotal target of the protective effects of IRF7 in vascular injury. Our findings strongly suggest that IRF7 is a novel modulator in vasculoproliferative diseases.

Methods

Mice

All of the animal protocols were approved by the Animal Care and Use Committee of Renmin Hospital of Wuhan University. The animal experiments were performed in accordance with the National Institutes of Health Guidelines for the Care and Use of Laboratory Animals (NIH Publication No. 80-23, revised in 1996). The SMC-specific IRF7 transgenic mice (IRF7-TG) were generated via the microinjection of full-length human IRF7 cDNA under the control of SMC-specific SM22α promoter into fertilized C57BL/6 embryos. The SMC-specific TG vector was constructed with a mouse SM22α promoter, a 5′-HA tag, and an SV40 polyA signal. The 1374-bp full-length IRF7 cDNA (Open Biosystem) was amplified with the primers 5′-GCCACCATG GAATTCGCTGAAGTGAGGGGGGTC-3′ (forward) and 5′-GTA TGGGTAGAATTCAGGCCACTGACCCAGGTC-3′ (reverse). Using the ligation-independent cloning (LIC) method, the amplified IRF7 cDNA was cloned into the SMC-specific TG vector between the *EcoRI* sites. The successful generation of IRF7 transgene was confirmed using Western blotting and PCR methods. The IRF7-KO mice (IRF7$^{-/-}$, C57BL/6 background, RBRC01420) were generously provided by Dr Taniguchi Tadatsugu (University of Tokyo)[20] and were confirmed using PCR analysis with the primers 5′-GTGGTACCCAGTCCTGCCCTCTTTATAATCT-3′, 5′-TC GTGCTTTACGGTATCGCCGCTCCCGATTC-3′, and 5′-AGTAGAT CCAAGCTCCCGGCTAAGTTCG TAC-3′. To generate SMC-specific ATF3 (ATF3-TG) mice, murine ATF3 cDNA was cloned using the primers 5′-GCCACCATGGAATTCATGATGCTTCAACATCCA GG-3′ (forward) and 5′- GTATGGGTAGAATTCGCTCTGCAATGTT CCTTCTT-3′ (reverse) and was inserted into fertilized embryos of C57BL/6 mice. The mice were genotyped via a PCR analysis of tail genomic DNA using the primers 5′-TGAGCCAAGCA GACTTCCAT-3′ (forward) and 5′-TATTTCTTTCTCG CCGCCT-3′ (reverse). The ATF3-KO mice were kindly provided by Tsonwin Hai (Ohio State University).[21] IRF7-TG mice and ATF3-TG mice were crossed to generate the SMC-specific-IRF7/ATF3-double-TG (DTG) mice, and the IRF7/ATF3-double-KO (DKO) mice were generated by crossing IRF7-KO mice and ATF3-KO mice. Both DTG and DKO mice were assessed using Western blot analyses. Only 10- to 12-week-old (25 to 30 g) males were used. The mice were exposed to a 12-hour light/dark cycle with controlled temperature and humidity. Food and water were provided ad libitum.

Generation of IRF7-KO Rats

Sprague-Dawley (SD) rats were purchased from Vital River Company (strain code: 101, Beijing, China). To create IRF7-KO SD rats, we used the region surrounding the intron 2/exon 3 junction of IRF7 as a candidate transcription activator-like effector (TALE) target site. The TALE repeats were designed using an online target designer (https://tale-nt.cac.cornell.edu/node/add/talen-old) and were constructed following the "unit assembly" method.[22] A 1400-bp *XbaI/XbaI* fragment encompassing the N- and C-terminal domains of TALE and the FokI nuclease domain was amplified via PCR from pCS2-FokI (AS/RR) using an appropriate primer pair: pCS2-F, 5′-GCT CTAGACCATGGCTCCAAAGAAGA-3′, and pCS2-R, 5′-CGTAA TACGA CTCACTATAG-3′. The fragment was cloned into the *NheI/XbaI* sites of a pcDNA3.1 vector under the control of a T7 promoter. The constructed vector was named pcDNA3.1-TALEN and was used instead of pCS2-TALEN. The TALEN expression plasmids were sequentially digested with *PmeI* restriction endonuclease (R0560L; New England Biolabs, Ipswich, MA) and proteinase K (Merck, Darmstadt, Germany) and were purified with phenol/chloroform to generate an RNase-free DNA template for in vitro transcription (mMessage mMachine T7 Ultra Kit, AM1345; Ambion, Austin, TX). Capped, polyA-tailed mRNAs were purified using the RNeasy Mini Kit (74104; Qiagen, Valencia, CA) following the manufacturer's instructions. TALEN mRNAs were diluted to 10 ng/μL with injection buffer (10 mmol/L Tris HCl/0.1 mmol/L

EDTA [pH 7.4]). Then, 2 pL of this solution was microinjected into the cytoplasm of one-cell-stage embryos using a FemtoJet 5247 microinjection system under standard conditions. The surviving embryos were then surgically transferred to pseudo-pregnant recipient females. F0 founder genotyping was performed by PCR amplification of a portion of the IRF7 gene spanning the TALEN target site, using the primers IRF7-F (5′-GCCGAAGTGAGGTGAGAACA-3′) and IRF7-R (5′-TATGG CCCTCCTCACCAGTT-3′). A 567-bp amplicon was denatured and re-annealed in NEB buffer 2. T7 endonuclease 1 (T7E1, 1 μL; NEB) was added to cleave the heteroduplex into approximately 350-bp and 210-bp nicked DNA fragments (45 minutes in a 37°C water bath). The surplus PCR products from the founders were TA cloned into T vectors according to the manufacturer's instructions (TaKaRa, D101A) and were sequenced using the M13-47 common primer. For the F1 and F2 generations, the primers IRF7-167-F (5′-ATAATCCGCCACA ACTCCTG3′) and IRF7-167-R (5′-GCACATCGGAAGTTGGTCTT-3′) were used to amplify the indel site. The PCR products were analyzed via 2% agarose gel electrophoresis in TBE buffer. The WT allele yielded a 167-bp amplicon, whereas the mutant allele yielded a 153-bp amplicon.

Murine Neointima Formation Model

The mouse carotid artery wire injury model has been described previously.[23] After being anesthetized with an intraperitoneal injection of sodium pentobarbital (80 mg/kg), the mice were subcutaneously injected with 1% lidocaine hydrochloride for local analgesia. The left carotid artery was exposed via a blunt-end dissection, and an 8-0 suture was used to ligate the external carotid artery proximal to the bifurcation. The internal and common carotid arteries were clamped to stop blood flow. A transverse incision was performed proximal from the suture around the external carotid artery, through which a guide wire (0.38 mm in diameter, No.C-SF-15-15, Cook, Bloomington) was introduced into the arterial lumen toward the aortic arch and was subsequently withdrawn 5 times using a rotating motion. After vascular injury, the guide wire and vascular clamps were successively removed to restore blood flow and the skin incision was then closed. The sham controls underwent the same procedures except for the vascular injury.

Carotid artery balloon injury was induced in male SD rats (300 g) as previously described.[24] In brief, after anesthetization, the left common carotid artery of the rat was exposed through a midline cervical incision. A Fogarty 2F catheter was advanced from just below the proximal edge of the omohyoid muscle to the carotid bifurcation three times (Baxter, McGaw Park, IL). To achieve constant and equal degrees of vessel wall injury in all the animals, we maintained a consistent balloon diameter and resistance during withdrawal. All of the procedures were performed by a single operator. The animals were subsequently processed for morphological and biochemical studies at specific time points after surgery.

Histological and Morphometric Analyses

At 0, 7, 14, or 28 days post-injury, the mice were euthanized through an intraperitoneal injection of sodium pentobarbital (150 mg/kg). The carotid arteries were harvested, fixed with 4% paraformaldehyde and paraffin-embedded. Serial 3-μm sections were cut from a ≈300-μm region at the bifurcation of the left carotid artery. For the rats, samples were collected at 0, 7, and 14 days post-injury, and serial 5-μm aortic sections were obtained. For the morphometric analysis, the sections were stained with hematoxylin and eosin (H&E) or Elastica van Gieson (EVG) staining after deparaffinization and rehydration. The indexes of neointima formation, intima area and the intima-to-media (I/M) ratio, were determined by a single observer who was blinded to the treatment protocols using Image-Pro Plus software (version 6.0; Media Cybernetics). A mean value was generated from 5 sections of each artery sample.

Immunofluorescence Staining

Immunofluorescence staining of the arterial sections was performed after antigen retrieval with high pressure for 5 minutes. Primary rat VSMCs were seeded onto coverslips in 6-well plates, fixed with fresh 4% paraformaldehyde for 15 minutes and permeabilized with 0.2% Triton X-100 in PBS for 5 minutes. The sections or slides were then blocked in PBS containing 10% goat serum and were incubated with primary antibodies overnight at 4°C. The primary antibodies used were rabbit anti-IRF7 (sc-9083; 1:100; Santa Cruz, Dallas, TX), mouse anti-SMA (ab7817; 1:100; Abcam, Cambridge, UK), mouse anti-PCNA (#2586; 1:100; Cell Signaling Technology, Beverly, MA), rat anti-7/4 (ab53457; 1:50; Abcam, Cambridge, UK), rabbit anti-CD3 (ab5690; 1:50; Abcam, Cambridge, UK), and rat anti-Mac3 (550292; 1:50; San Diego, CA). The sections were washed with PBS and incubated with the appropriate secondary antibodies at 37°C for 1 hour. The employed secondary antibodies included Alexa Fluor 568-conjugated goat anti-rabbit IgG (A11011; Invitrogen, Carlsbad, CA), Alexa Fluor 488-conjugated goat anti-mouse IgG (A11001; Invitrogen), Alexa Fluor 568-conjugated goat anti-mouse IgG (A11004; Invitrogen), Alexa Fluor 568-conjugated goat anti-rabbit IgG (A11011; Invitrogen, Carlsbad, CA), and Alexa Fluor 555-conjugated anti-rat IgG (#4417; Cell Signaling Technology, Beverly, MA). Nuclei were stained with 4′,6-diamidino-2-phenylindole (DAPI). Images were acquired using a fluorescence microscope (Olympus DX51) with the DP2-BSW software (version 2.2). Image-Pro Plus software was used to calculate the integrated optical density (IOD) values.

RNA Isolation and Quantitative Real-time PCR

Total RNA was extracted from mouse carotid artery tissue using TRIzol reagent (Roche; 11667165001; Indianapolis, IN). The cDNA was synthesized using a Transcriptor First Stand cDNA Synthesis Kit (Roche; 04897030001, Indianapolis, IN). The quantitative real-time PCR analysis were performed in 20-μL volumes using the LightCycler 480 SYBR Green I Master Mix, 04887352001, Roche and LightCycler® 480 Real-time PCR system (Roche) following the manufacturer's instructions. The primer pairs that were used for Collagen I 5′-TGGTACATCAGCCCGAAC-3′ (forward) and 5′-GTCAGCTGG ATAGC GACA-3′ (reverse); Collagen III 5′-CCCAACCCAGAG ATCCCATT-3′ (forward); and 5′-GAAGCACAGGAGCAGGTGT AGA-3′ (reverse). The samples were quantified by normalizing the gene expression level to that of the standard housekeeping β-actin gene and expressed as relative mRNA levels compared with the internal control.

Cell Culture and Construction of Adenoviral Vectors

Human aortic smooth muscle cells (HASMCs) were obtained from the American Type Culture Collection (ATCC). Primary VSMCs were isolated and purified from thoracic aortas of male C57BL/6, IRF7-TG and IRF7-KO mice or SD rats through enzymatic digestion. All of the cells were maintained in Dulbecco's modified Eagle's medium (DMEM)/F12 supplemented with 10% fetal bovine serum (FBS, SV30087.02, HyClone) and 1% penicillin-streptomycin at 37°C in a humidified 5% CO_2 incubator. Cells from passages 3 to 5 were used in the experiments.

Adenoviruses harboring sequences encoding rat IRF7 and a truncated IRF7 lacking the ID domain (Admutant) were generated. To overexpress IRF7, the entire coding region of the rat IRF7 gene was placed into a replication-defective adenoviral vector under the control of the cytomegalovirus promoter. The truncated IRF7 adenovirus was generated using the following primers: 5′-CTGCACCGCGGTGCAA GAGCCCC GTGAGGGTGTGTCTTCCCTG-3′ (forward), and 5′-CAGGGAAG ACA CACCCTCACGGGGCTCTTGCACCGCGGTGCA-3′ (reverse). Recombinant adenoviruses were generated using the AdEasy vector kit (Stratagene, La Jolla, CA). Inserts were cloned into the pShuttle-CMV vector. Plasmids were recombined with the pAdEasy backbone vector according to the manufacturer's instructions and were transfected into HEK293 cells using FuGENE transfection reagent (E2312, Roche, Indianapolis, IN). Recombinant adenoviruses were plaque-purified, titered to 10^9 PFU/mL, and verified via restriction digestion. To knockdown IRF7 expression, three rat shIRF7 constructs were purchased from SABiosciences (KR54505G) to construct AdshIRF7 adenoviruses. AdshRNA was used as a non-targeting control. The human ATF3-overexpressing adenovirus was obtained from Applied Biological Materials Inc (000186A). A similar adenoviral vector encoding the GFP gene was used as a control. The cells were infected with adenoviruses in a diluted medium at a multiplicity of infection (MOI) of 50 for 24 hours.

VSMC Proliferation Assay

VSMC proliferation was determined using a BrdU incorporation assay (Roche Diagnostics, Mannheim, Germany). Quiescent VSMCs (5×10^3/well) were growth-arrested in a 96-well microplate. After being grown to 60% confluence, the VSMCs were exposed to serum-free medium for 24 hours, and were then stimulated with 20 ng/mL PDGF-BB (ProSpec, Rehovot, Israel) for 48 hours. BrdU was added to the culture medium for the final 2 hours and the incorporation levels were measured according to the manufacturer's instructions.

Western Blotting

Western blotting analysis was performed as previously described.[25] Cellular and mouse tissue proteins were exposed to radioimmunoprecipitation assay (RIPA) buffer (50 mmol/L Tris-HCl [pH 7.6], 150 mmol/L NaCl, 1% NP-40, 0.5% sodium deoxycholate, and 0.1% SDS), homogenized on ice and centrifuged. The supernatants were resolved via 10% SDS-PAGE and were transferred to PVDF membranes (Millipore). The membranes were blocked with Tris-buffered saline (TBS) containing 5% non-fat milk and were incubated with the following primary antibodies: rabbit anti-IRF7 (sc-9083; 1:200; Santa Cruz), mouse anti-PCNA (#2586; 1:1000; Cell Signaling Technology), rabbit anti-Cyclin D1 (#2978; 1:1000; Cell Signaling Technology), rabbit anti-NF-κB p65 (#4764; 1:1000; Cell Signaling Technology), rabbit anti-phosphorylated-NF-κB p65 (ser536) (BS4138; 1:1000; Bioworld), mouse anti-IκBα (#4814; 1:1000; Cell Signaling Technology), mouse anti-phosphorylated IκBα (BS4105; 1:1000; Bioword), rabbit anti-TNFα (#3707; 1:1000; Cell Signaling Technology), goat anti-IL-6 (AF-406-NA; 1:500; R&D System), goat anti-Collagen type I (sc-8784; 1:1000; Santa Cruz), goat anti-Collagen type III (sc-8781; 1:1000; Santa Cruz), rabbit anti-ATF3 (sc-188; 1:200; Santa Cruz), and mouse anti-GAPDH (MB001; 1:10 000; Bioworld).

Plasmid Constructs

Recombinant enhanced green fluorescent protein (EGFP)-myc-IRF7 was constructed by cloning the coding region of the human IRF7 gene between the *BamHI* and *XhoI* sites of psi-EGFP-myc-C1. HA-IRF7 was PCR amplified with IRF7-5′ and IRF7-3′, which are shown in Table. The pmCherry-IRF7 construct was generated by amplifying the coding region of the IRF7 gene and subcloning it into pmCherry-C1. To obtain the

Table. The Primers Used for Making the Constructs

Primer Name	Primer Sequence (5′ to 3′)
IRF7-5′	CGCGGATCCATGGCCTTGGCTCCTGAGAG
IRF7-3′	CCGCTCGAGCTAGGCGGGCTGCTCCAGCT
IRF7-N1-3′	CCGCTCGAGCTAGCTGGGGGTCGTCTCTACTG
IRF7-C1-5′	CGCGGATCCAGCCCCGGGCCCCAGCCCGC
IRF7-ID-5′	CGCGGATCCGAGCCCAGCCCAGGGGCGCT
IRF7-ID-3′	CCGCTCGAGCTAACGCTGCGTGCCCTCTAGGT
IRF7-dID-5′	CTGCACCGCGGTGCAAGAGCCCCGTGAGGGTGTGTCTTCCCTG
IRF7-dID-3′	CAGGGAAGACACACCCTCACGGGGCTCTTGCACCGCGGTGCA
ATF3-5′	CGCGGATCCATGATGCTTCAACATCCAGGC
ATF3-3′	CCGCTCGAGTTAGCTCTGCAATGTTCCTTC
ATF3-N-3′	CCGCTCGAGTTACTCAGACTTGGTGACTGACA
ATF3-dN-5′	CGCGGATCCGCGGCCCCTGAAGAAGATGA
ATF3-C-5′	CGCGGATCCTTGATATACATGCTCAACCT

ATF3 indicates activating transcription factor 3; IRF7, interferon regulatory factor 7.

IRF7 fragments consisting of residues 1–246, 245–503, and 284–467, HA-IRF7 was PCR amplified with IRF7-5′/IRF7-N1-3′, IRF7-C1-5′/IRF7-3′, and IRF7-ID-5′/IRF7-ID-3′, respectively.

The IRF7 deletion mutant lacking residues 284–467 was generated using a 2-step PCR-based mutagenesis procedure with HA-IRF7 as the template. In the first step, 2 partially overlapping fragments were PCR-amplified using the primer sets IRF7-dID-5′/IRF7-3′ and IRF7-5′/IRF7-dID-3′. The fragments were annealed and were used as the template for the second PCR amplification, in which the primers IRF7-5′ and IRF7-3′ were used to amplify the full-length mutant IRF7. The resulting mutant PCR product was digested with *BamHI* and *XhoI* and was ligated into psi-EGFP-myc-C1 to obtain EGFP-myc-IRF7Δ284-467.

The Flag-ATF3 and EGFP-myc-ATF3 constructs were generated by amplifying the coding region of the ATF3 gene (using primers ATF3-5′ and ATF3-3′) from HA-ATF3 and subcloning the amplicon into psi-Flag-C1 and psi-EGFP-myc-C1, respectively. To obtain the ATF3 fragments consisting of residues 1–80, 81–181 and 141–181, Flag-ATF3 was PCR amplified using the primer sets ATF3-5′/ATF3-N-3′, ATF3-dN-5′/ATF3-3′ and ATF3-C-5′/ATF3-3′, respectively. The products were digested with *BamHI* and *XhoI* and were ligated into psi-Flag-C1 to create an in-frame fusion with the Flag. The primers used to create these constructs are shown in Table. All of the plasmids were verified via sequencing.

Immunoprecipitation

Immunoprecipitation was performed to investigate the association between IRF7 and ATF3. Cultured 293T cells were cotransfected with Flag-ATF3 and EGFP-myc-IRF7 for 48 hours, collected and lysed in immunoprecipitation buffer (20 mmol/L Tris-HCl [pH 8.0], 150 mmol/L NaCl, 1 mmol/L EDTA, and 0.5% NP-40) containing a protease inhibitor cocktail (Roche). The resulting cell homogenates were incubated for 20 minutes at 4°C, followed by centrifugation at 13 000*g* for 15 minutes. After that, a complex containing the sample (500 μL), antibody (1 μg) and protein A/G-agarose beads (10 μL, 11719394001, 11719386001; Roche) was incubated on a rocking platform overnight at 4°C. Subsequently, the immunoprecipitates were washed with cold IP buffer, separated via SDS-PAGE, and subject to Western blotting using specific primary antibodies.

Glutathione S-Transferase (GST) Pull-Down Assay

The GST fusion protein, GST-IRF7, was purified from 10 mL of *E. coli* after IPTG induction and was immobilized on glutathione-Sepharose 4B beads (GE Healthcare Bio-Sciences AB). The GST-IRF7 beads were then incubated with Flag-ATF3-transfected 293T cell lysates in immunoprecipitation buffer for 4 hours at 4°C. The GST tag was used as a negative control in identical conditions. The samples were analyzed via Western blotting using anti-Flag antibodies.

Confocal Microscopy

The 293T cells were inoculated in a gelatin-coated 24-well plate. After cotransfection with pmCherry-IRF7 and EGFP-myc-ATF3 for 48 hours, the cells were fixed in 4% paraformaldehyde for 15 minutes, permeabilized with 0.2% Triton X-100 and incubated in Image-IT™ FX signal enhancer (I36933, Invitrogen) for 30 minutes. Following washing with TBS-T and DAPI

staining, the slides were mounted using mounting solution (D2522; Sigma). Images were obtained with a confocal laser-scanning microscope (Fluo View 1,000; Olympus).

Luciferase Reporter Assay

The human PCNA promoter plasmid (NC_000020.10, 5108429-5107227, negative strand) was purchased from the RIKEN BRC DNA Bank (Japan) and was subcloned into the pGL3-basic vector (Promega, Madison) between the *XhoI* and *HindIII* restriction sites. The CRE elements of PCNA were predicted using Genomatix MatInspector online software (http://www.genomatix.de/). CRE-luc was obtained from Applied Biological Materials Inc (000174A). Primary RASMCs were cultured in a 24-well plate and were co-infected with the indicated recombinant adenoviruses. Twenty-four hours later, the cultured cells were exposed to PDGF-BB (20 ng/mL), and lysed by adding 100 μL of passive lysis buffer (PLB; Promega) per well at indicated time points. After centrifugation, the supernatants were collected and assessed for luciferase activity using a Single-Mode SpectraMax® Microplate Reader.

Chromatin Immunoprecipitation

For the ChIP assay, mouse SMCs were grown to 60% confluence and serum-starved for 24 hours, quiescent cells were treated with 20 ng/mL of PDGF-BB for 30 minutes. Then the cells were harvested, fixed with 1% formaldehyde for 10 minutes, and washed with ice-cold PBS. The cells were then sonicated to generate DNA fragments, which were immunoprecipitated using anti-ATF3 (SC188-X) and normal rabbit IgG (CST; 2729S) followed by protein G-magnetic beads (Invitrogen; 10004D). The precipitated DNA was recovered via phenol/chloroform extraction and amplified through RT-PCR using specific primers for PCNA: 5′-AGCCCCGCCTTT GCATAC-3′ (forward) and 5′-CTACAGCGACAACTACCA ACCCT-3′ (reverse).

Statistical Analyses

The data analysis was performed using the SPSS software, version 17.0 (SPSS Inc, Chicago, IL). The data are presented as the mean values±standard errors (SEM). After confirming that the data passed the normality test for parametric analyses, the differences between 2 groups were determined using the independent-samples *t* test, the differences among multiple groups were determined using a 1-way or 2-way analysis of variance (ANOVA) followed by the least significant difference (LSD) test or Tamhane's T2 post-hoc test. A probability value (*P*) of less than 0.05 was considered to be statistically significant.

Results

IRF7 Expression is Significantly Decreased in Response to Carotid Injury

To evaluate whether IRF7 was involved in neointima formation, we first measured the IRF7 expression in VSMCs, the most prominent cells in the formation and development of intimal hyperplasia. As shown in Figure 1A, under physiological conditions, IRF7 immunofluorescence was specifically found to overlap with VSMCs in carotid arteries. Subsequently, a classic wire injury-induced neointima formation model was established in C57BL/6 mice (Figure 1B) to assay the alteration of IRF7 expression in response to vascular injury. The in situ immunofluorescence staining and Western blotting indicated that, accompanied by the progressive thickening of the intima, the expression of IRF7 was gradually decreased between 14 and 28 days post-injury and was even negligible at 28 days (Figures 1C and 1D). Simultaneously, the VSMC proliferation markers, PCNA and Cyclin D1, were strikingly increased (Figure 1D), which suggested that the transcription factor IRF7 is involved in the pathophysiology of VSMC proliferation and neointima formation.

PDGF-BB, a growth factor promotes the dedifferentiation and proliferation of SMCs,[26,27] was employed to stimulate rat aortic smooth muscle cells (RASMCs) and human aortic smooth muscle cells (HASMCs) to mimic the vascular injury model in vitro. Western blotting showed that the level of IRF7 decreased dramatically in a time-dependent manner in response to PDGF-BB (20 ng/ml) (Figures 1E and 1F), confirming the potentially functional role of IRF7 in the proliferation of SMCs.

IRF7 Overexpression Represses Neointima Formation and VSMC Proliferation

Owing to the evidence indicating that VSMCs play a prominent role in neointima formation and that IRF7 is robustly expressed and regulated in VSMCs in response to vascular injury, SMC-specific IRF7 transgenic mice (IRF7-TG) were generated under the control of the SM22α promoter to elucidate the role of IRF7 in regulating neointima formation, particularly in VSMCs (Figure 2A). Four IRF7-TG lines were successfully generated, and line 4 exhibited the most significant increase (7.19-fold) in IRF7 expression compared with the non-transgenic controls (NTG) (Figure 2B). This line was therefore used for further experimentation. The baseline intima area and the intima to media (I/M) ratio values were comparable between the IRF7-TG mice and NTG littermates (Figure 2C). However, after carotid artery wire injury, the IRF7-TG mice presented significant reductions in the increases of the intima area and the I/M ratio compared with the NTG controls at 14 and 28 days post-injury (Figure 2C). PCNA immunofluorescence staining and Western blotting analyses were performed to determine the level of

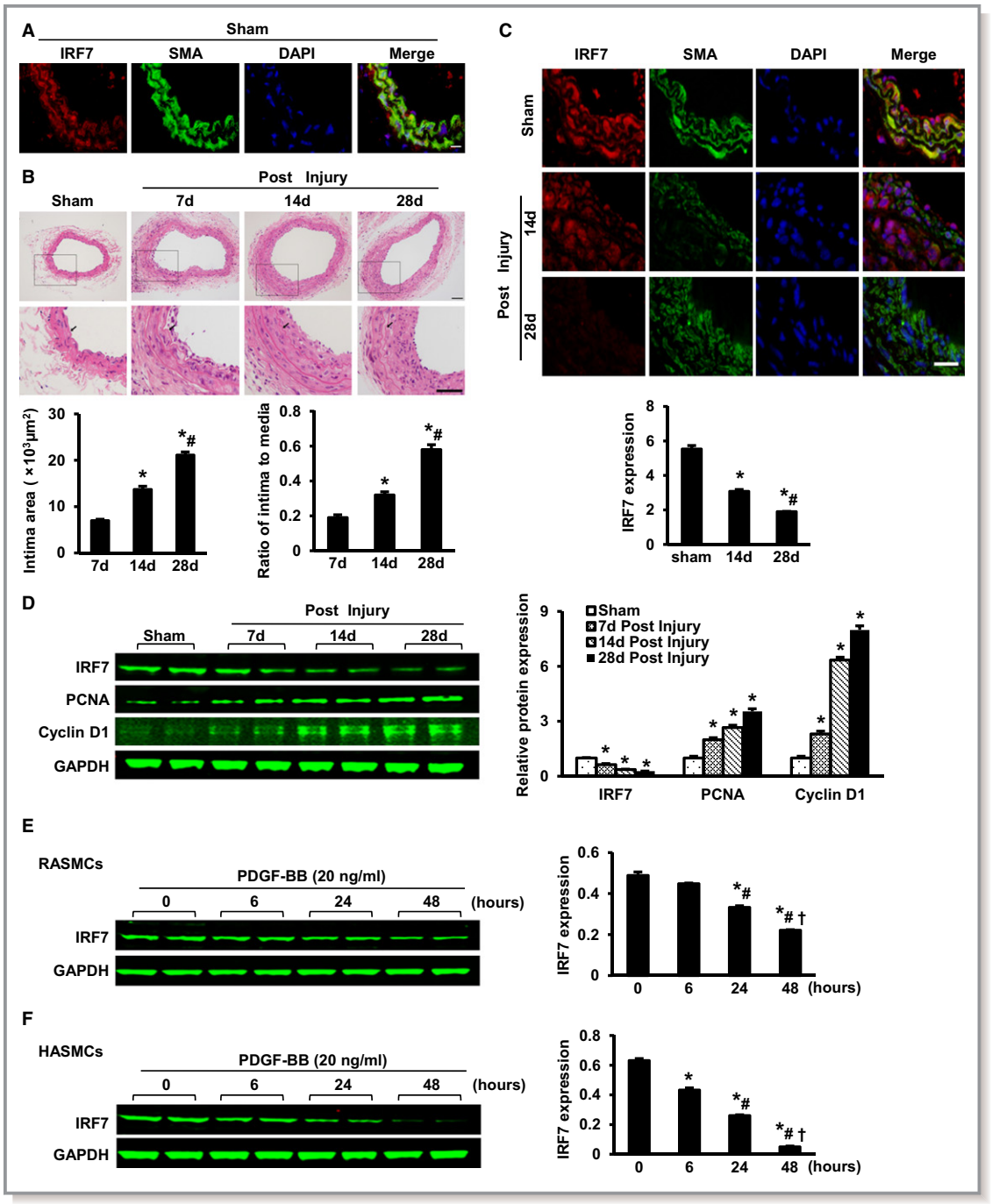

Figure 1. IRF7 expression is decreased after carotid injury or PDGF-BB stimulation. A, Costaining of IRF7 (red) and SMA (green) in a mouse carotid artery under physiological conditions. (n=4). Scale bar: 50 μm. B, Hematoxylin and eosin staining of carotid artery sections from wild-type mice at the indicated time points following wire injury. Scale bar: 50 μm. Bottom panel: quantification of the intima area and I/M ratio at the indicated times (n=9 for 7-day injured group, n=10 for 14-day injured group, n=12 for 28-day injured group). **P*<0.05 vs day 7; #*P*<0.05 vs day 14. C, Injury-induced alterations in the expression of IRF7 (red) and SMA (green) evaluated via immunostaining (n=4 for sham group, n=3 for 14-day injured group, n=3 for 28-day injured group). **P*<0.05 vs the sham group; #*P*<0.05 vs day 14. D, Western blotting analysis of the expression of IRF7, PCNA and Cyclin D1 in carotid arteries at 7, 14, and 28 days after injury (n=3 samples for each time point, 3 to 4 carotid arteries were collected as 1 sample). **P*<0.05 vs the sham group. E and F, Western blotting analysis of IRF7 protein levels in rat aortic smooth muscle cells (RASMCs, E) and human aortic smooth muscle cells (HASMCs, F) at 0, 6, 24, and 48 h after PDGF-BB (20 ng/mL) administration. The expression levels were normalized to that of GAPDH and were quantified. (n=3). **P*<0.05 vs the untreated group, #*P*<0.05 vs the 6 hours post-stimulation group, †*P*<0.05 vs the 24 hours post-stimulation group. In (B) to (F), Data are represented as the mean±SEM. IRF7 indicates interferon regulatory factor 7; PCNA, proliferating cell nuclear antigen; PDGF, platelet-derived growth factor.

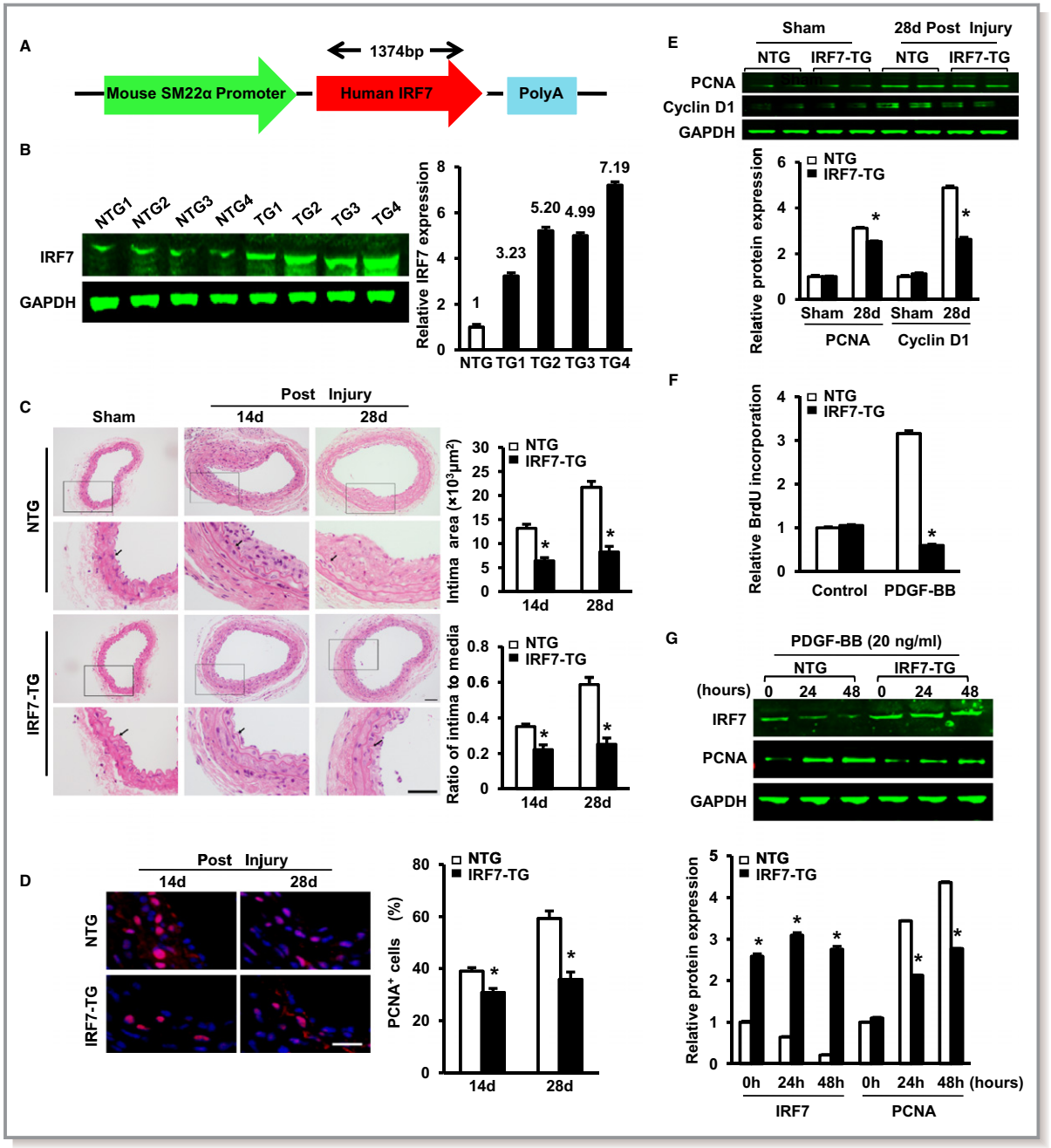

Figure 2. IRF7 overexpression represses neointima formation and VSMC proliferation in response to carotid injury. A, Schematic representation of the transgene construct. B, Representative Western blotting of the expression of IRF7 in the carotid arteries of NTG and IRF7-TG mice (n=4 samples for each genotype, 3 to 4 carotid arteries were collected as 1 sample). C, Hematoxylin and eosin staining of the carotid arteries of NTG and IRF7-TG mice at 14 and 28 days post-injury. Scale bar: 50 μm. Right panel: quantitative analysis of the intima area and I/M ratio (n=7 to 9 per group at 14 days post-injury, n=9 per group at 28 days post-injury). *P<0.05 vs NTG mice. D, Immunofluorescence staining for PCNA (red) in the carotid arteries of NTG and IRF7-TG mice at 14 and 28 days post-injury. Scale bar: 50 μm. Right panel: quantification of PCNA-positive cells in the carotid arteries (n=3 to 4 per group at 14 or 28 days post-injury). *P<0.05 vs NTG mice. E, Western blotting of PCNA and Cyclin D1 in the carotid artery at 28 days post-injury. Bottom panel: quantification of PCNA and Cyclin D1 (n=3 samples per group, 3 to 4 carotid arteries were collected as 1 sample). *P<0.05 vs NTG mice. F, BrdU incorporation of primary VSMCs isolated from NTG and IRF7-TG mice after PDGF-BB (20 ng/mL) stimulation (n=5 to 6). *P<0.05 vs NTG VSMCs. G, Western blotting of IRF7 and PCNA in NTG and IRF7-TG VSMCs after PDGF-BB (20 ng/mL) stimulation. Bottom panel: quantification of IRF7 and PCNA. *P<0.05 vs NTG VSMCs. In (B) to (G), Data are represented as the mean±SEM. IRF7 indicates interferon regulatory factor 7; NTG, non-transgenic; PCNA, proliferating cell nuclear antigen; VSMCs, vascular smooth muscle cells.

cellular proliferation in the neointima, with the result that the number of PCNA-positive cells and the PCNA and Cyclin D1 protein expression were markedly lower in the IRF7-TG mice than in their NTG littermates after injury (Figures 2D and 2E).

Consistent with the in vivo results, our in vitro investigation demonstrated that when treated with PDGF-BB (20 ng/ml), primary IRF7-TG VSMCs showed dramatically lower proliferation levels, as indicated by striking reductions in BrdU incorporation (Figure 2F) and PCNA expression (Figure 2G), compared with the NTG VSMCs. Additionally, although PDGF-BB downregulated the level of IRF7, the IRF7 expression appeared to be high and stable at each time point after PDGF-BB stimulation in the IRF7-overexpression VSMCs, which might contribute to the reductions in the elevated proliferation and related factors. Accordingly, we determined that the repression of neointima formation was, at least partially, due to the regulatory effects of IRF7 on VSMC proliferation.

IRF7 Deficiency Exacerbates Neointima Formation and VSMC Proliferation

Given the evidence that IRF7 overexpression suppressed intimal thickening in response to vascular injury, we evaluated whether IRF7 deficiency was deleterious to neointima formation and VSMC proliferation. Carotid wire injury was performed on IRF7-KO and WT littermates. In contrast to IRF7-TG mice, the IRF7-KO mice exhibited increases in the intima area and the I/M ratio, which were significantly higher compared with the WT controls at different time points (14 and 28 days) after injury (Figure 3A). The proliferation markers PCNA and Cyclin D1 were dramatically elevated in the IRF7-KO carotid arteries in response to vascular injury, as determined by PCNA immunofluorescence staining and Western blotting analysis (Figures 3B and 3C).

To elucidate the effect of IRF7 deficiency on VSMC proliferation in vitro, we isolated primary VSMCs from IRF7-KO and WT mice and treated them with PDGF-BB (20 ng/mL). BrdU incorporation revealed that IRF7-KO VSMCs and WT VSMCs exhibited indistinguishable levels of proliferation without PDGF-BB stimulation. However, in the presence of PDGF-BB, IRF7-KO VSMCs had significantly higher levels of BrdU incorporation (Figure 3D) and dramatically increased PCNA protein levels, as shown by Western blotting (Figure 3E), compared with WT VSMCs. Accordingly, IRF7 deficiency may promote VSMC proliferation, thereby exacerbating neointima formation.

IRF7 Protects Against Inflammation and Connective Tissue Deposition in Response to Carotid injury

Inflammation plays an important role in neointima formation after vascular injury.[28] Previous work and our recent study showed that IRF7 modulates the inflammatory response in various cell types and diseases, such as cardiac hypertrophy and diet-induced obesity and insulin resistance.[15,16] To further evaluate whether IRF7 protects against neointima formation through inflammation, we examined the inflammatory cell infiltration and inflammatory state in the IRF7-TG and IRF7-KO mice in response to wire injury. Immunofluorescence staining revealed that inflammatory cells, including neutrophils, T lymphocytes, and macrophages, were significantly increased in the carotids of the IRF7-KO mice at 7 days post-injury (Figure 4A). Western blotting showed that the expression levels of p-p65, p-IκBα, TNF-α, and IL-6 were decreased in the IRF7-TG mice at 7 days post-injury, and an opposite effect was observed in the IRF7-KO mice compared with the WT controls (Figures 4B and 4C). These results are consistent with our previous study and demonstrate that IRF7 protects against inflammation by targeting NF-κB signaling after vascular injury.

Additionally, we evaluated connective tissue deposition in IRF7-TG and IRF7-KO mice after wire injury; this deposition also contributes to the progression of neointima formation.[3,29] At 28 days post-injury, the results showed that the mRNA expression of Collagen I and Collagen III was decreased in the IRF7-TG mice and increased in the IRF7-KO mice compared with the NTG or WT controls (Figure 4D). Consistent with this finding, the protein expression of Collagen I, Collagen III, and Fibrillin-1 was also downregulated in the IRF7-TG mice and upregulated in the IRF7-KO mice compared with the NTG or WT controls (Figure 4E). These results demonstrate that IRF7 suppresses connective tissue deposition in response to carotid injury.

The Regulatory Effects of IRF7 on PDGF-BB-induced VSMC Proliferation are ATF3 Dependent

Although the protective effects of IRF7 on neointima formation have been firmly verified, as mentioned above, the underlying mechanism involved in this functional regulation has yet to be elucidated. For the purpose of this investigation, yeast two-hybrid screening was performed. IRF7 was used as bait to identify its potential interacting proteins, and a clone encoding a specific transcription factor, ATF3, was identified as an interesting candidate (Figure 5A). To confirm the protein–protein interaction between IRF7 and ATF3, we transfected 293T cells with EGFP-myc-IRF7 and Flag-ATF3 plasmids and performed a co-immunoprecipitation (co-IP) experiment. The results showed that IRF7 readily interacted with ATF3 and vice versa (Figure 5B). A GST pull-down experiment further confirmed that Flag-ATF3 was pulled down with GST-tagged IRF7 but not with GST (Figure 5C). Additionally, confocal fluorescence microscopy demonstrated that the fluorescence signals of IRF7 and ATF3 in the nuclei of 293T

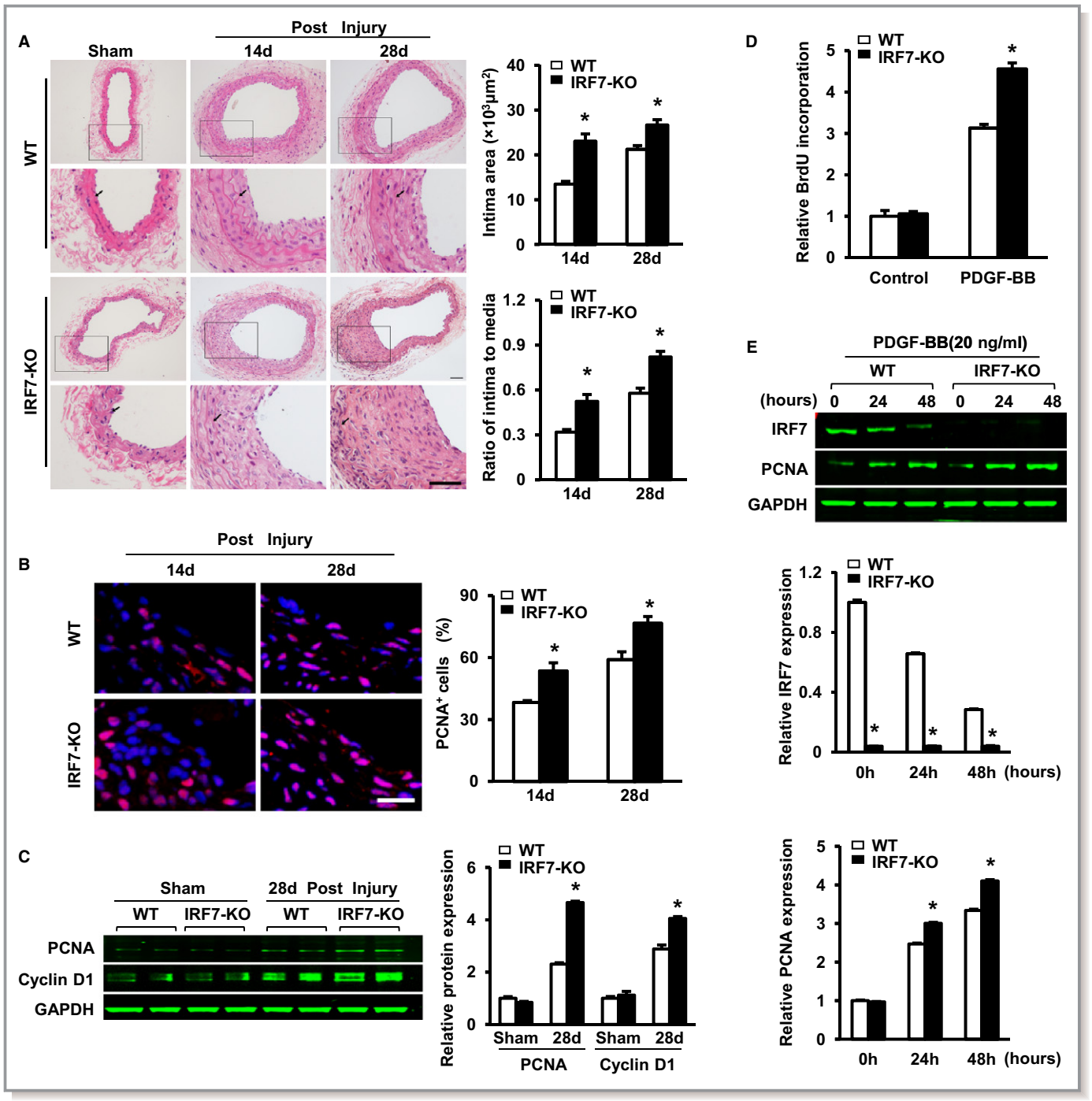

Figure 3. IRF7 deficiency promotes neointima formation and VSMC proliferation in response to carotid injury. A, Hematoxylin/eosin-stained WT and IRF7-KO carotid arteries at 14 and 28 days after injury. Scale bar: 50 μm. Right panel: quantitative analysis of the intima area and I/M ratio in histological sections (n=7 to 9 per group at 14 days post-injury, n=8 to 9 per group at 28 days post-injury). **P*<0.05 vs WT mice. B, Immunofluorescence staining for PCNA (red) at 14 and 28 day post-injury. Scale bar: 50 μm. Right panel: quantification of PCNA-positive cells in the carotid arteries (n=3 to 4 per group at 14 day post-injury, n=4 per group at 28 days post-injury). **P*<0.05 vs WT mice. C, Western blotting of PCNA and Cyclin D1 in the carotid arteries at 28 days post-injury. Right panel: quantification of PCNA and Cyclin D1 via Western blotting (n=3 samples per group, 3 to 4 carotid arteries were collected as 1 sample). **P*<0.05 vs WT mice. D, BrdU incorporation in primary VSMCs isolated from WT and IRF7-KO mice after PDGF-BB (20 ng/mL) stimulation (n=5 to 6). **P*<0.05 vs WT VSMCs. E, Western blotting of PCNA in WT and IRF7-KO VSMCs after PDGF-BB (20 ng/mL) stimulation. Bottom panel: quantification of IRF7 and PCNA via Western blotting analysis. **P*<0.05 vs WT VSMCs. In (A) to (E), Data are represented as the mean±SEM. IRF7 indicates interferon regulatory factor 7; KO, knock out; PCNA, proliferating cell nuclear antigen; PDGF, platelet-derived growth factor; VSMCs, vascular smooth muscle cells.

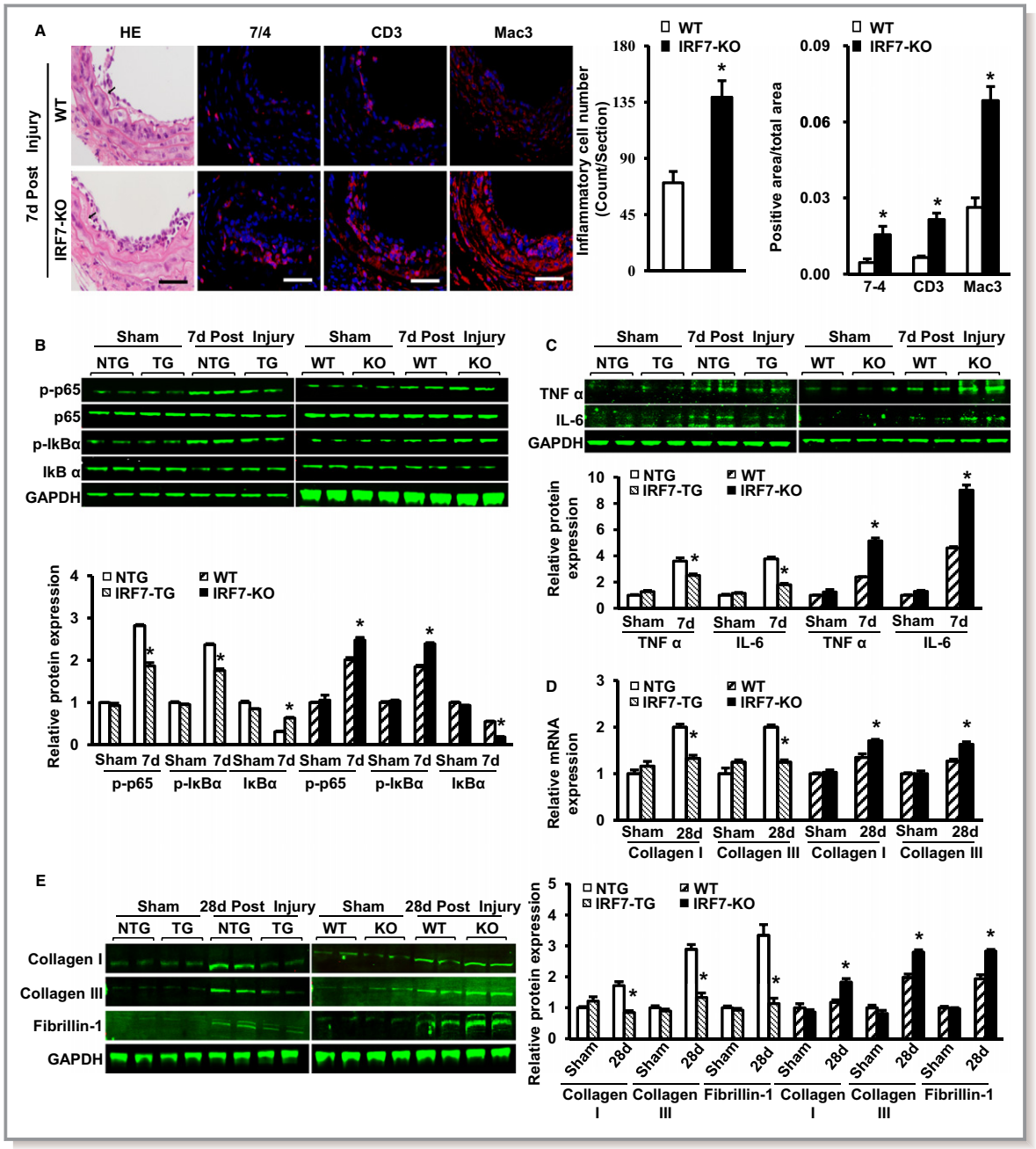

Figure 4. IRF7 protects against inflammation and connective tissue deposition in response to carotid injury. A, Left panel: immunofluorescence staining for 7/4, CD3 and Mac3 (red) in the carotids of WT and IRF7-KO mice at 7 days post-injury. Scale bar: 50 μm. Right panel: quantitative analysis of the total inflammatory cell number and positive area of 7/4, CD3 and Mac3 to total area. **P*<0.05 vs WT mice (n=3 to 4). B, Top panel: representative Western blotting of p-p65, p65, p-IκBα, and IκBα in the carotid arteries of NTG, IRF7-TG, WT, and IRF7-KO mice at 7 days post-injury. Bottom panel: quantification of p-p65, p-IκBα and IκBα via Western blotting. **P*<0.05 vs NTG or WT mice. (n=3 samples per group, 3 to 4 carotid arteries were collected as 1 sample). C, Top panel: representative Western blotting of TNF-α and IL-6 in the carotid arteries of NTG, IRF7-TG, WT and IRF7-KO mice at 7 days post-injury. Bottom panel: quantification of TNF-α and IL-6 via Western blotting. **P*<0.05 vs NTG or WT mice (n=3 samples per group, 3 to 4 carotid arteries were collected as 1 sample). D, Real-time PCR showing the expression of Collagen I and Collagen III in the carotid arteries of NTG, IRF7-TG, WT and IRF7-KO mice at 28 days post-injury (n=6). **P*<0.05 vs NTG or WT mice. E, Left panel: representative Western blotting of Collagen I, Collagen III, and Fibrillin-1 in the carotid arteries of NTG, IRF7-TG, WT, and IRF7-KO mice at 28 days post-injury. Right panel: quantification of Collagen I, Collagen III, and Fibrillin-1 via Western blotting (n=3 samples per group, 3 to 4 carotid arteries were collected as 1 sample). In (B through C) and (E), the protein expression levels were normalized to GAPDH. In (A) to (E), all of the values are presented as the mean values±SEM. IRF7 indicates interferon regulatory factor 7; KO, konck out; NTG, non-transgenic; PCNA, proliferating cell nuclear antigen; PCR, polymerase chain reaction; PDGF, platelet-derived growth factor; VSMCs, vascular smooth muscle cells.

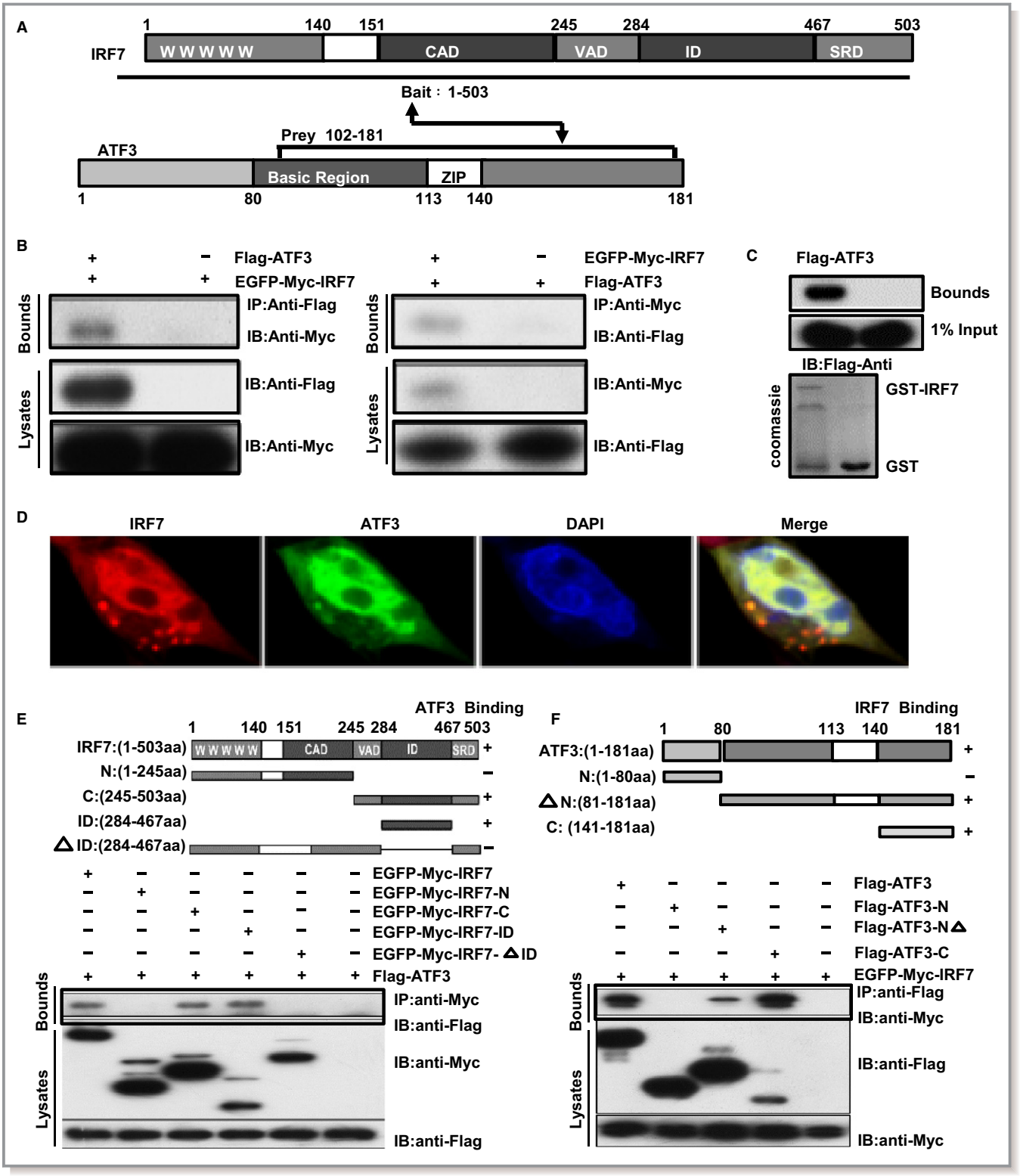

Figure 5. Interaction between IRF7 and ATF3. A, Schematic diagram of the IRF7 protein structure; a.a. 1–503 was used as bait to examine a potential interaction with a.a. 1–181 of ATF3. B, Co-immunoprecipitation (IP) of IRF7 and ATF3 in 293T cells. The cells were transfected with EGFP-Myc-tagged IRF7 and Flag-tagged ATF3. The lysates were immunoprecipitated with anti-Myc and were analyzed by immunoblotting using anti-flag antibodies. C, Immunoblot analysis of GST-pull-down assays of Flag-tagged ATF3 with GST or GST-IRF7. D, Colocalization of IRF7 (red) and ATF3 (green) in the nucleus. The nuclei were stained with DAPI (blue). E and F, Schematic diagrams of the IRF7 (E) and ATF3 (F) deletion mutants. Bottom panel: mapping the ATF3-binding region of IRF7 (E) and the IRF7-binding region of ATF3 (F) via Co-IP. ATF3 indicates activating transcription factor 3; EGFP, enhanced green fluorescent protein; GST, glutathione s-transferase; IRF7, interferon regulatory factor 7.

cells transfected with pCherry-IRF7 and pEGFP-ATF3 colocalized well (Figure 5D), which provides further evidence for a relationship between IRF7 and ATF3. To identify the specific region of the interaction between IRF7 and ATF3, we generated various truncations of IRF7 and ATF3. Co-IP experiments revealed that the intermediate domain (ID, a.a. 284–467) of IRF7 and the C-terminal domain (a.a. 141–181) of ATF3 interacted with ATF3 and IRF7, respectively (Figures 5E and 5F).

IRF7 Inhibits ATF3-Induced PCNA Transcription

The finding that IRF7 interacts with ATF3 prompted us to investigate the mechanism by which ATF3 mediates the IRF7 effect on VSMC proliferation. Considering that ATF3 is a transcription factor, we employed the Genomatix MatInspector online software to search the potential targets of ATF3. Of note, we observed three ATF3 binding sites in the promoter of PCNA, a key regulator of cellular proliferation. To examine whether IRF7 affects ATF3 transactivation, we introduced a luciferase reporter driven by three tandem repeats of an ATF3 consensus response element (3×CRE) into RASMCs. We observed that AdshIRF7 significantly enhanced the increase in CRE-luc activity induced by PDGF-BB, which was blocked by AdshATF3 infection (Figure 6A). This result indicates that IRF7 inhibits ATF3 transactivation. To examine whether this effect applies to the inhibition of PCNA expression by IRF7, we cloned the

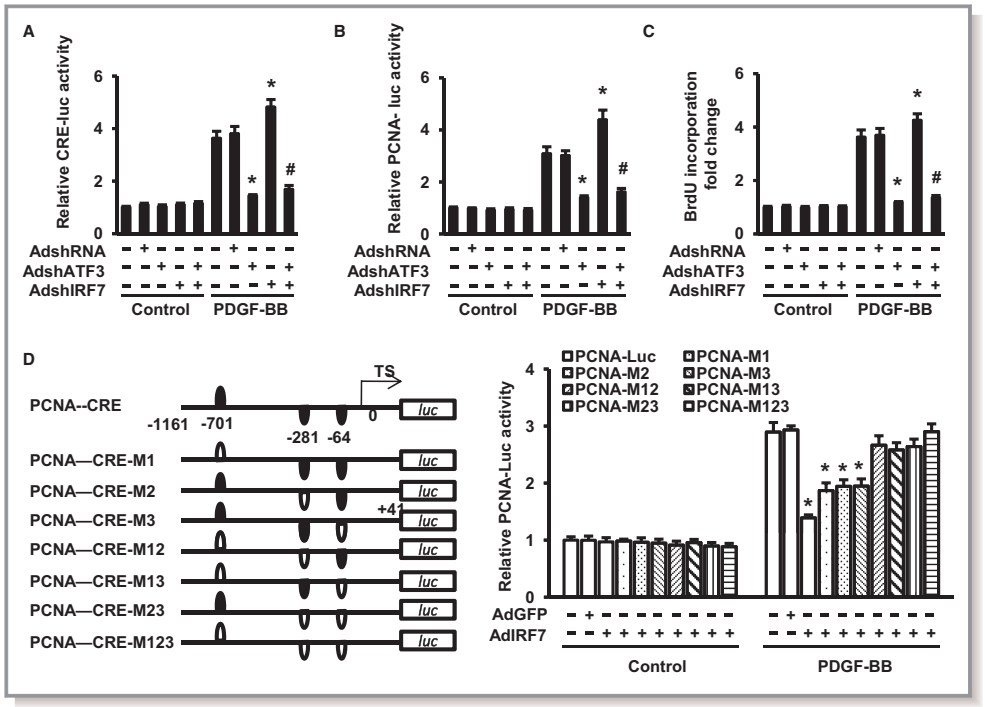

Figure 6. The regulatory effects of IRF7 on PDGF-BB-stimulated VSMC proliferation are dependent on ATF3 and its binding to the CRE element on the PCNA promoter. A and B, Luciferase activity assay of CRE-luc (A) and PCNA-luc (B) in RASMCs infected with AdshRNA, AdshATF3, AdshIRF7, or AdshATF3+AdshIRF7 after PDGF-BB (20 ng/mL) stimulation. *P<0.05 vs AdshRNA, $^{\#}P$<0.05 vs AdshIRF7 (n=3). C, BrdU incorporation into RASMCs after infection with AdshRNA, AdshATF3, AdshIRF7, or AdshATF3+AdshIRF7 with PDGF-BB stimulation (20 ng/mL). *P<0.05 vs AdshRNA, $^{\#}P$<0.05 vs AdshIRF7 (n=3). D, Schematic diagrams of 7 types of mutant PCNA-luc reporter constructs. Right panel: luciferase activity assay of PCNA in RASMCs transfected with various mutant PCNA-luc constructs and AdIRF7 after PDGF-BB (20 ng/mL) stimulation. *P<0.05 vs PCNA-luc+AdGFP (n=3). E, Changes in the binding ability of ATF3 to the PCNA promoter in NTG and IRF7-TG mouse VSMCs upon PDGF-BB (20 ng/mL) stimulation were analyzed using the ChIP qPCR technique. *P<0.05 vs NTG VSMCs. F and G, Luciferase activity assay of CRE-luc (F) and PCNA-luc (G) in RASMCs after infection with AdGFP, AdATF3, AdIRF7, AdIRF7 mutants, AdATF3+AdIRF7, or AdATF3+AdIRF7 mutants with PDGF-BB (20 ng/mL) stimulation. *P<0.05 vs AdGFP, $^{\#}P$<0.05 vs AdATF3, $^{\dagger}P$<0.05 vs AdATF3+AdIRF7 (n=3). H, BrdU incorporation into RASMCs after infection with AdGFP, AdATF3, AdIRF7, AdIRF7 mutants, AdATF3+AdIRF7, or AdATF3+AdIRF7 mutants with PDGF-BB stimulation (20 ng/mL). *P<0.05 vs AdGFP, $^{\#}P$<0.05 vs AdATF3, $^{\dagger}P$<0.05 vs AdATF3+AdIRF7 (n=3). Data are represented as the mean±SEM. ATF3 indicates activating transcription factor 3; PDGF, platelet-derived growth factor; RASMCs, rat aortic smooth muscle cells; VSMCs, vascular smooth muscle cells.

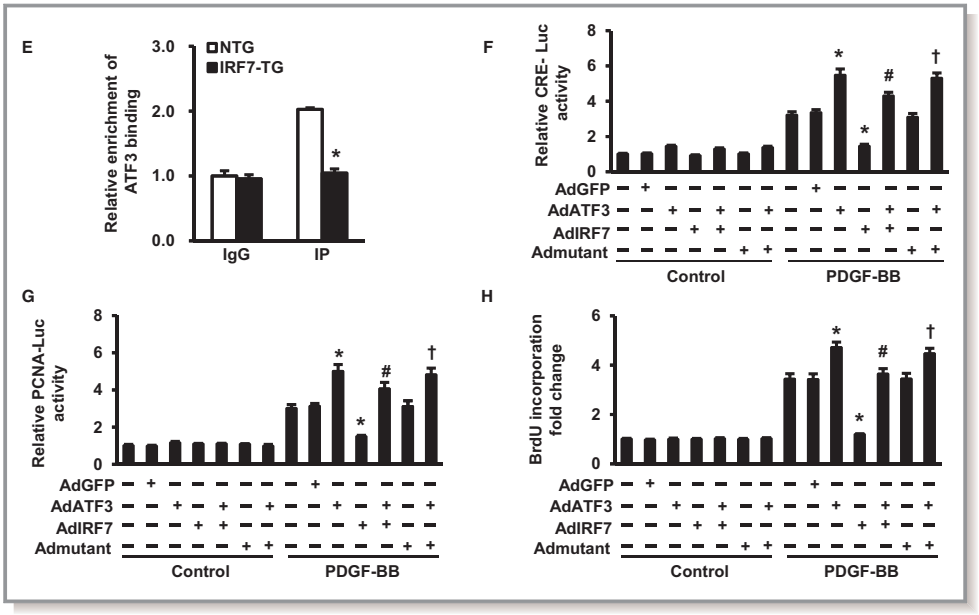

Figure 6. Continued.

human PCNA promoter sequence, inserted it upstream of the luciferase reporter gene and examined the transcriptional induction of PCNA promoter. Similar to the CRE-luc results, the induction of PCNA-luc activity by AdshIRF7 was abolished by AdshATF3 infection (Figure 6B). The in vitro RASMC proliferation was evaluated by BrdU labeling. We further observed that AdshATF3 prevented the induction of BrdU incorporation by AdshIRF7 infection (Figure 6C). Collectively, these results suggest that ATF3 is responsible for the effects of IRF7 on PCNA expression and VSMC proliferation.

To verify that ATF3 is a bona fide mediator of IRF7 on PCNA expression, we mutated the three ATF3 consensus response elements (CREs) in the human PCNA promoter separately (M1, M2, M3) and simultaneously (M12, M13, M23, M123) (Figure 6D, left panel). Upon PDGF-BB stimulation, AdIRF7 infection inhibited WT PCNA-luc activity. When we mutated 2 or 3 of the CREs in the PCNA promoter simultaneously (M12, M13, M23, M123), AdIRF7 infection failed to inhibit PCNA-luc activity (Figure 6D, right panel). Chromatin immunoprecipitation (ChIP) further confirmed that PCNA was a direct target of ATF3, with the results indicating that ATF3 could bind to the PCNA promoter region, whereas this response was inhibited in IRF7-TG VSMCs (Figure 6E). These results indicate that ATF3 directly targets PCNA and is required for the inhibition of PCNA expression by IRF7.

Because ATF3 is responsible for the inhibition of PCNA by IRF7, we next sought to examine whether this effect is realized through the direct interaction between IRF7 and ATF3. As expected, AdIRF7 infection suppressed the CRE-luc and PCNA-luc activities, which were enhanced by AdATF3 infection (Figures 6F and 6G). However, when we infected the cells with AdmutantIRF7, which lacked the region responsible for the interaction with ATF3, the CRE-luc, and PCNA-luc activities were not suppressed (Figures 6F and 6G). Additionally, AdIRF7 infection inhibited BrdU incorporation, whereas AdmutantIRF7 infection failed to do so (Figure 6H). All of these results indicate that IRF7 inhibits ATF3-induced PCNA expression and RASMC proliferation via the direct interaction of IRF7 and ATF3.

The Regulatory Effects of IRF7 on Neointima Formation and VSMC Proliferation are ATF3 Dependent

To investigate whether ATF3 was required for the neointima formation and VSMC proliferation modulated by IRF7 in vivo, we generated SMC-specific ATF3 transgenic mice (ATF3-TG) containing murine ATF3 cDNA (543 bp) under the control of SM22α promoter (Figure 7A). The IRF7/ATF3-DTG mice were obtained by crossing IRF7-TG mice with ATF3-TG mice (Figure 7B). Concurrently with the gain-of-function experiment, IRF7/ATF3-DKO mice were obtained by crossing ATF3-KO with IRF7-KO mice to investigate whether ATF3 was responsible for the observed effects of IRF7 ablation (Figure 7C). The genotypes of these mice were confirmed via Western blotting analysis (Figures 7B and 7C). Next, we subjected NTG, ATF3-TG, IRF7-TG, and DTG mice to carotid injury. The intima area, the I/M ratio, and the number of PCNA-positive cells were significantly increased in the ATF3-TG mice at 28 days post-injury; these increases were

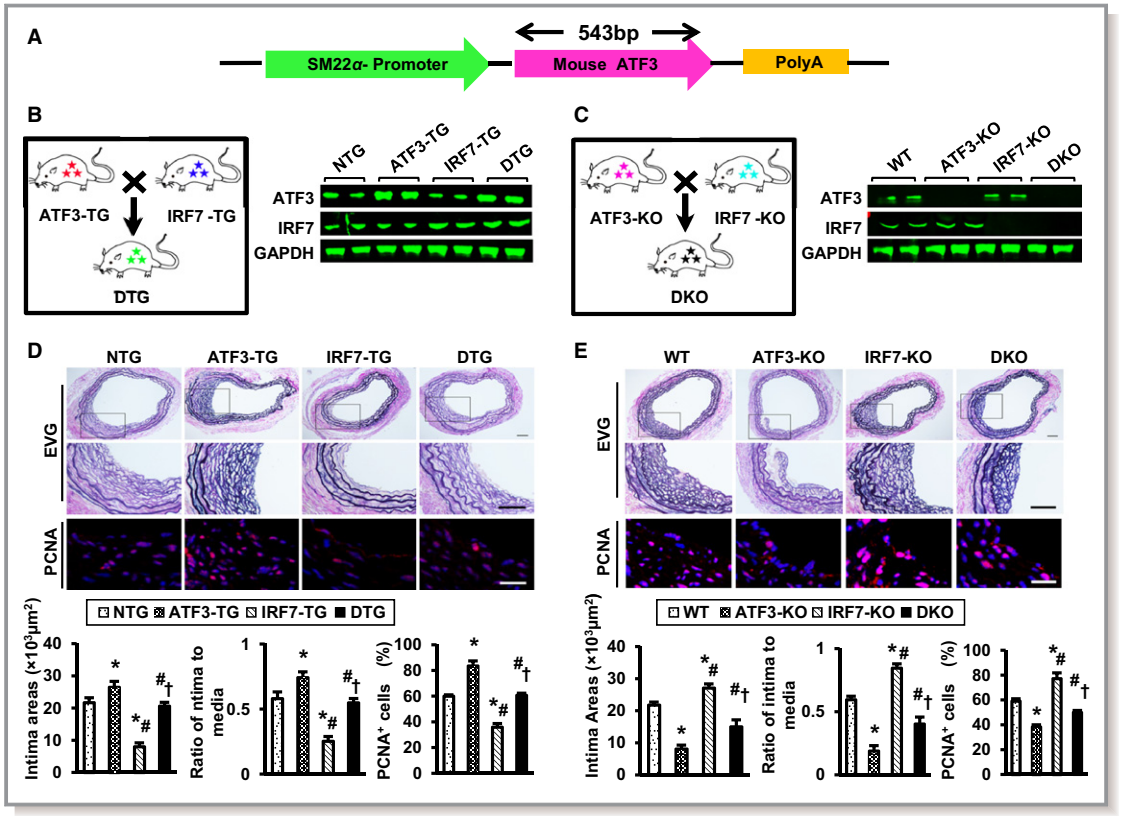

Figure 7. IRF7/ATF3-DTG and IRF7/ATF3-DKO abolish IRF7-TG and IRF7-KO regulated neointima formation and VSMC proliferation. A, A construct containing full-length murine ATF3 cDNA under the control of a minimal SM22α promoter. B and C, Schematic diagrams of DTG (B) and DKO (C) mice and the expression of IRF7 and ATF3 detected via Western blotting (n=4 samples per group, 3 to 4 carotid arteries were collected as 1 sample). D, Elastin-van Gieson (EVG)-stained NTG, ATF3-TG, IRF7-TG and DTG carotid arteries and the immunofluorescence staining of PCNA at 28 days post-injury. Bottom panel: quantitative analysis of the intima area and I/M ratio in the histological sections (n=5 to 7 per group) and PCNA-positive cells in the neointima and media (n=3 to 4 per group). Scale bar: 50 μm. *P<0.05 vs NTG mice, $^{\#}P$<0.05 vs ATF3-TG, $^{\dagger}P$<0.05 vs IRF7-TG. E, Elastin-van Gieson (EVG)-stained WT, ATF3-KO, IRF7-KO and DKO carotid arteries and immunofluorescence staining of PCNA at 28 days post-injury. Bottom panel: quantitative analysis of the intima area and I/M ratio in the histological sections (n=5 to 7 per group) and PCNA-positive cells (n=3 to 4 per group). Scale bar: 50 μm. *P<0.05 vs WT mice, $^{\#}P$<0.05 vs ATF3-KO, $^{\dagger}P$<0.05 vs IRF7-KO. F through H, CRE-luciferase activity (F), PCNA-luciferase activity (G), and BrdU incorporation (H) were examined in AdGFP- or AdIRF7-infected primary VSMCs of ATF3-TG mice after PDGF-BB (20 ng/mL) stimulation. *P<0.05 vs NTG VSMCs infected with AdGFP, $^{\#}P$<0.05 vs NTG VSMCs infected with AdIRF7 (n=3). I through K, CRE-luciferase activity (I), PCNA-luciferase activity (J) and BrdU incorporation (K) in AdshRNA or AdshIRF7 infected primary VSMCs of ATF3-KO mice after PDGF-BB (20 ng/mL) stimulation. *P<0.05 vs WT VSMCs infected with AdshRNA, $^{\#}P$<0.05 vs WT VSMCs infected with AdshIRF7 (n=3). In (D) to (K), data are represented as the mean±SEM. ATF3 indicates activating transcription factor 3; IRF7, interferon regulatory factor 7; KO, knock out; NTG, non-transgenic; PCNA, proliferating cell nuclear antigen; VSMCs, vascular smooth muscle cells.

dramatically reduced by IRF7-TG. Interestingly, in DTG mice, the inhibitory effects of IRF7 overexpression on neointima formation were abolished (Figure 7D). As expected, in the IRF7-KO mice subjected to vascular injury, Elastin-van Gieson (EVG) staining revealed that the increased intima area and I/M ratio after vascular injury in the IRF7-KO mice were largely restored by ATF3 deficiency (Figure 7E). Moreover, the VSMC proliferation indicated by the immunofluorescence staining for PCNA was also significantly decreased in DKO mice compared with that of IRF7-KO after carotid injury (Figure 7E).

Subsequently, we infected primary VSMCs isolated from ATF3-TG mice with AdIRF7 (MOI=50) in vitro and observed that in the presence of PDGF-BB, IRF7 overexpression significantly decreased the CRE-luc and PCNA-luc activities and VSMC proliferation in WT VSMCs. Consistent with the in vivo results, the inhibitory effect of IRF7 overexpression was remarkably alleviated in ATF3-overexpressing VSMCs (Figures 7F, 7G, and 7H). Similarly, compared with the WT primary VSMCs, the AdshIRF7-infected ATF3-KO VSMCs displayed significantly lower activities of CRE-luc, PCNA-luc, and BrdU incorporation in the presence of PDGF-BB

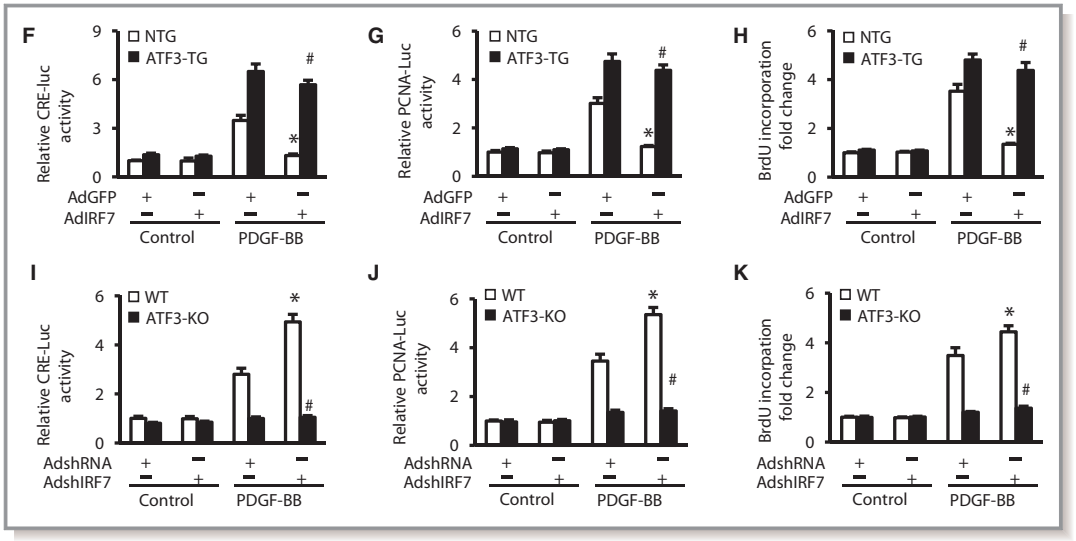

Figure 7. Continued.

(Figures 7I, 7J, and 7K). These findings demonstrate that IRF7 modulation of neointima formation and VSMC proliferation in response to carotid injury and PDGF-BB stimulation is dependent on ATF3.

IRF7 Deficiency in Rats Exacerbates Neointima Formation After Balloon Injury and VSMC Proliferation In Vitro

To further determine whether IRF7 is involved in neointima formation in the rat model, a classic carotid balloon injury model was well established in SD rats. We generated an IRF7-KO rat strain using TALEN technology to confirm the role of IRF7 in rat intimal hyperplasia. The region surrounding the intron 2/exon 3 junction of the rat IRF7, as the target site, was genetically disrupted using TALENs (Figure 8A). Among all of the examined embryos, 8 live-born offspring were produced and screened for the targeted disruption of IRF7 using the T7E1 assay. Of the 8 offspring, 5 founders were identified with cleaved products (Figure 8B), which contained 1 different mutant allele. The PCR products from 2 randomly selected founders were then TA cloned and sequenced to verify the precise location of the indel mutations (Figure 8C). One founder (rat #2-5, carrying an allele with a 14-bp deletion) was randomly chosen to establish the $IRF7^{\triangle 14/+}$ and $IRF7^{\triangle 14/\triangle 14}$ rat strains. Consequently, a novel IRF7-KO rat strain was successfully generated by mating the heterozygous rat siblings carrying the targeted mutation. The rat genotypes were verified via PCR and agarose gel electrophoresis (Figure 8D) and Western blotting (Figure 8E).

Subsequently, the generated IRF7-KO rats and a control group were subjected to the classic carotid balloon injury model in parallel. Similar to the results observed in mice, at 7 and 14 days post-injury, an increased intima area and I/M ratio were observed in IRF7-KO rats compared with controls (Figure 8F). Correspondingly, the effects of IRF7 deficiency on VSMC proliferation were evaluated using immunohistochemistry and Western blotting analysis, with the results indicating that the expression levels of PCNA and Cyclin D1 were significantly increased in IRF7-knockout rats post-injury (Figures 8G and 8H). Complementing our findings in mice, the aggravating effects of IRF7 deficiency on balloon injury-induced intimal thickening in the novel rat line further validated the crucial regulatory function of IRF7 in neointima formation and VSMC proliferation.

Discussion

This study represents the first detailed investigation of the regulatory effects and underlying mechanisms of IRF7 in neointima formation. Our results demonstrated that IRF7, a novel crucial regulatory factor in intimal hyperplasia, was significantly downregulated in carotid VSMCs in both in vivo and in vitro models mimicking vascular injury. The SMC-specific overexpression of IRF7 alleviated vascular injury-induced VSMC proliferation and intimal hyperplasia, whereas IRF7 ablation exacerbated this phenotype. Furthermore, the detrimental effects of IRF7 deletion on vascular injury were confirmed in a novel rat IRF7-KO strain. Mechanistically, ATF3 was identified as a transcription factor that is indispensable for modulating the effects of IRF7 and that promotes neointima formation and VSMC proliferation.

IRF7, a protein first isolated as a transcriptional factor that binds to the Epstein-Barr virus *Bam*HI Q promoter, is predominantly expressed in lymphoid cells and participates in innate and adaptive immunity.[20,30,31] As a master regulator

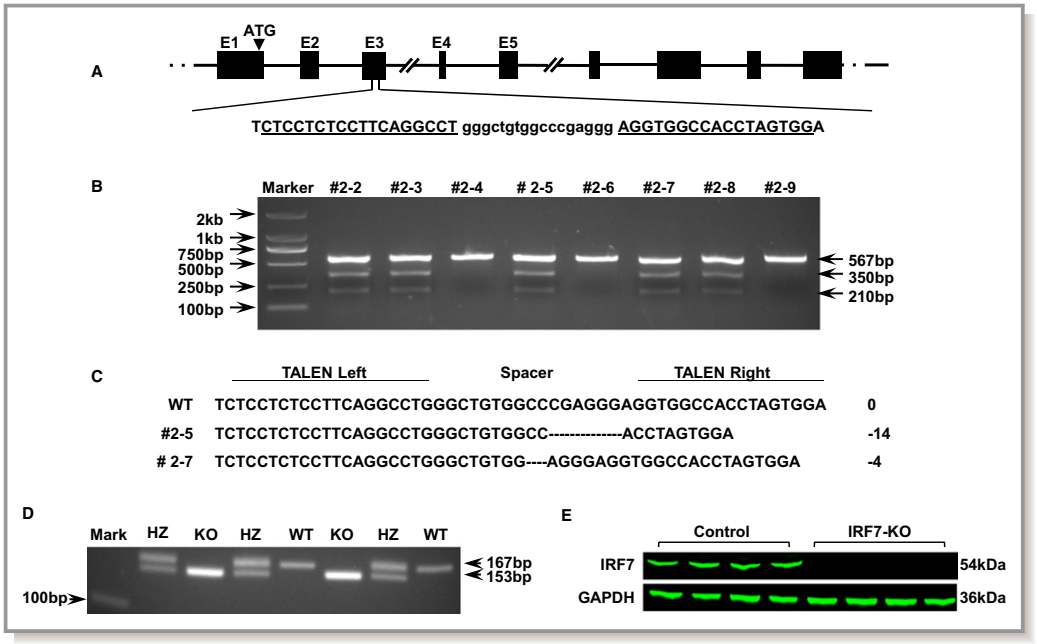

Figure 8. Generation of IRF7-KO rats via TALEN-mediated gene inactivation and the detrimental effect of IRF7-KO on balloon injury-induced neointimal hyperplasia in rats. A, A pair of TALENs was designed to target the region surrounding the intron 2/exon 3 junction of rat IRF7. The sequence shown is the TALEN target; the TALEN-binding sequence is in uppercase letters, and the digestion site is in lowercase letters. B, Agarose gel photograph of the T7 endonuclease 1 digestion assay showing the digestion products of the predicted size from WT SD (567 bp) and mutant rats (350 and 210 bp). The arrows indicate the sizes of the bands. C, WT DNA sequence of IRF7 with TALEN-binding sites and spacer or the sequences determined from the cloned PCR products from founder rats (#2–5 and #2–7). One founder (rat #2–5, carrying an allele with a 14-bp deletion) was randomly chosen to establish the $IRF7^{\triangle 14/+}$ and $IRF7^{\triangle 14/\triangle 14}$ rat strains. D, F2 rats were generated by mating F1 heterozygotes ($IRF7^{\triangle 14/+}$, HZ) and were genotyped via PCR and agarose gel electrophoresis. The 167-bp band represents the WT allele, and the 153-bp band represents the mutant allele. E, Western blotting results showing the expression of IRF7 in the carotid arteries of WT and IRF7-KO rats (n=4 samples). F, Representative cross-sections of hematoxylin/eosin-stained carotid arteries of control and IRF7-KO rats without injury (Sham) or at 7 and 14 days after balloon injury. Scale bar: 50 μm. Bottom panel, quantitative analysis of the intima area and I/M ratio (n=7 to 8 per group at 7 days post-injury, n=7 to 8 per group at 14 days post-injury). *P<0.05 vs the control rats. G, Representative immunohistochemical staining of PCNA in cross-sections of the carotid arteries of control and IRF7-KO rats at 7 and 14 days post-injury. Scale bar: 50 μm. (n=4 per group). H, Western blotting results showing the expression of PCNA and Cyclin D1 in the carotid arteries of control and IRF7-KO rats without injury (Sham) and at 14 days post-injury. Bottom panel: quantification of the normalized protein levels (n=3 samples). *P<0.05 vs the control. In (F) and (H), Data are represented as the mean±SEM. IRF7 indicates interferon regulatory factor 7; KO, knock out; HZ, heterozygote; PCNA, proliferating cell nuclear antigen; PCR, polymerase chain reaction; PDGF, platelet-derived growth factor; VSMCs, vascular smooth muscle cells.

of type I IFN-dependent immune responses, IRF7 has been shown to protect against pathogenic infections and to participate in many diseases, primarily autoimmune disorders and cancer.[20,32,33] It has been demonstrated that IRF7 is involved in the miR-155-induced CD8 (+) T cell response,[34] hepatitis C infection,[35] and inflammatory sequelae of antiviral responses;[36] IRF7 also acts as a crucial effector of breast cancer migration[37] and brain tumor progression and heterogeneity.[32] Although the regulatory roles of IRF7 in immunity and cancer have been extensively investigated, the details of IRF7 activation in VSMCs and neointima formation remained obscure until now. In this study, IRF7 expression decreased significantly in response to wire injury in vivo and after treatment with PDGF-BB in vitro, implying that IRF7 may play an important role in neointima formation. Additionally, the strikingly opposite results in IRF7-TG and IRF7-KO mice demonstrate that IRF7 is a novel effector that protects against intimal hyperplasia; this protection is at least partially attributed to the suppression of VSMC proliferation.

With the development of rat genome sequencing and the emergence of promising genetic engineering methods, rat models have become powerful tools to mimic human diseases and to further identify targets and signaling pathways underlying disease phenotypes, which are aided by the

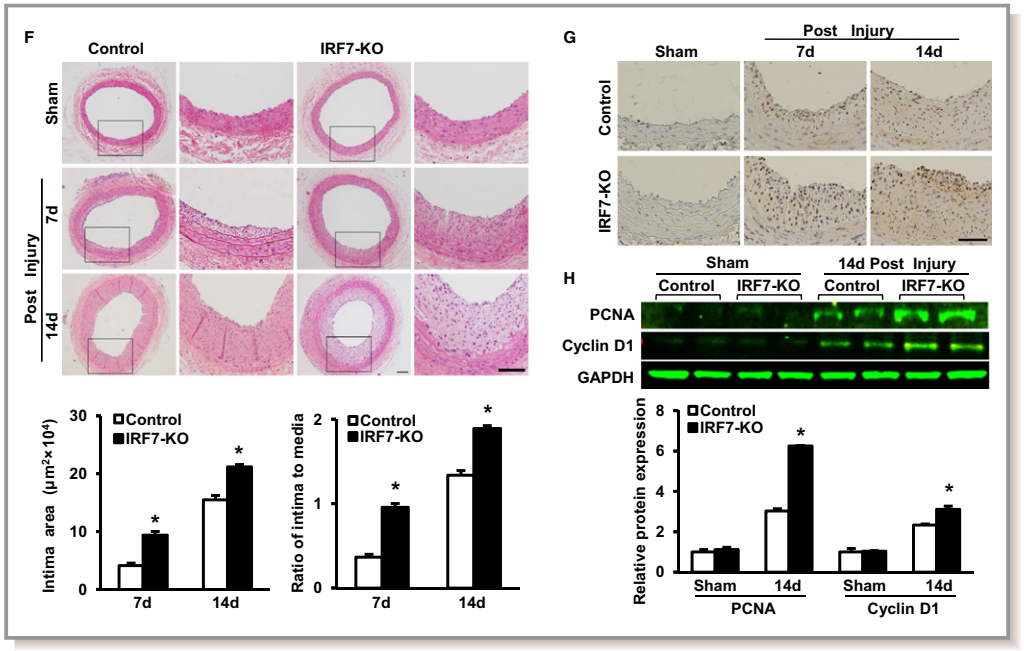

Figure 8. Continued.

response of rats to treatment and their higher similarities to the human physiology compared with mice.[38] Balloon injury-induced intimal hyperplasia in rats is a classic model that is suitable for laboratory research.[39–41] Therefore, we attempted to validate the protection of IRF7 in neointima formation via a balloon injury-induced rat model. However, the creation of an IRF7-KO rat had previously failed due to the limitations of available genetic techniques. Recently, TALEN has emerged as an efficient tool for creating genetically engineered models in various species via genome editing and the introduction of targeted double-strand breaks (DSBs).[42] This method circumvents the requirement for embryonic stem cells and opens up the application of gene targeting for many species other than mice, such as rats. Tesson[43] and Ferguson et al[44] reported the successful deletion of Igm and TLR4, respectively, in rats using this promising technology. In the present study, a pair of TALENs targeting a specific region of IRF7 was designed, and an IRF7-knockout rat strain carrying a 14-bp deletion allele was produced with a high success rate; this strain represents a valuable technical resource for the further elucidation of the IRF7 function and molecular events. The novel rat strain was used to further confirm the aggravating effects of IRF7 deficiency on neointima formation. To the best of our knowledge, this study is the first direct and clear report on the effects of IRF7 on neointimal hyperplasia in both mouse and rat models.

Vascular injury triggers versatile molecular events, particularly VSMC proliferation, leading to the thickening of blood vessels.[3] However, the critical targets and signaling pathways in VSMC proliferation remain problematic. Accumulating evidence has demonstrated that ATF3, a member of the ATF/CREB family of transcription factors, can be induced by various extra- and intracellular stimuli and may encode additional transcription factors that determine cell fates, ie, death, survival, proliferation, and inflammatory responses.[45–47] It has been reported that active ATF3 promotes the proliferation of several cell types, eg, Hodgkin lymphoma and malignant prostate cancer cells,[48,49] leukemia cells,[50] hepatocytes,[51] and renal medulla cells,[52] via treatment with growth-stimulating factors, such as serum, epidermal growth factor, fibroblast growth factor, or PDGF-BB.[53,54] In the vascular system, recent studies have indicated that ATF3 primarily regulates vascular endothelial cell apoptosis and inflammation[55] and the migration of VSMCs.[56] The pleiotropic functions of ATF3 were attributed to its formation of homodimers or heterodimers with ATF2, c-Jun or other cellular transcription factors through the CRE element.[50] However, the biological significances and the mechanism by which ATF3 induces VSMC proliferation are not thoroughly understood. Using yeast two-hybrid screening, we identified that ATF3 is an IRF7-interacting protein. Additionally, the IRF7/ATF3-DTG and IRF7/ATF3-DKO mice exhibited reductions in the phenotypes of IRF7-TG and IRF7-KO mice, respectively, relating to VSMC proliferation and intimal hyperplasia, indicating that ATF3 is required for IRF7-modulated neointima formation. Furthermore, according to the luciferase reporter assay results, the proliferation marker PCNA was identified as a direct downstream target of ATF3, and the identified CRE sites are necessary for the binding of ATF3 to PCNA and for IRF7-regulated VSMC proliferation.

We demonstrated that IRF7 expression was decreased in response to carotid injury and that IRF7 inhibited VSMC proliferation and neointima formation. However, previous work and our recent study revealed the involvement of excess IRF1 and IRF8 in VSMC proliferation and neointima formation after carotid injury.[11,57]Although the IRFs displayed opposite changes in their expression in these studies, they led to a similar effect on VSMC proliferation in response to vascular injury. The reason for this finding is most likely that some cytokines or transcriptional factors involved in neointima formation have an opposite effect on IRF expression, such as PDGF-BB, which can reduce IRF7 expression but increases IRF8 expression in VSMCs.[11] By contrast, although IRFs have opposite expression trends in response to carotid injury, they have distinct targets through which they modulate VSMC proliferation; for example, IRF1 targets P21, IRF8 targets SRF, and IRF7 targets PCNA, which may lead to a similar effect on VSMC proliferation.[11,57] Using gain of function and loss of function experiments we demonstrated that IRF3, IRF7 and IRF8 all played important roles in neointima formation after wire injury through different mechanisms,[11,58] indicating that the IRFs are crucial regulators in the neointima formation. However, based on our current findings, we could not conclude which IRF is more important. Additionally, the cooperation or competition of different transcription factors of the IRF family at the DNA-binding level has been demonstrated in in vitro studies.[59] It is therefore possible that interplay exists among these different IRFs and combines to regulate VSMC functions and neointima formation in response to vascular injury. Understanding the nature of cross-talk between these signaling pathways is helpful to understand the molecular basis of the roles of the IRF family in neointima formation after vascular injury. We do not know whether cross-talk and interactions exist among these IRFs after vascular injury, and we are currently conducting research in this area.

In the present study, we employed a mouse carotid wire-injury model to evaluate the effect of IRF7 on neointima formation. Wire injury has been a common method for inducing carotid injury in mice for the past 20 years. The technique completely removes the endothelium with a flexible wire and leads to neointima formation.[60] Although the subsequent artery remodeling mimics the neointima formation in humans after percutaneous coronary intervention (PCI) treatment, this model cannot completely reflect the pathogenesis of vascular injury in the clinical setting. To further expand our findings in clinical applications, additional research is necessary to evaluate the relationship of IRF7 expression with VSMC proliferation and neointima formation in clinical specimens.

In conclusion, we identified IRF7 as a novel modulator of neointima formation using both in vivo mice and rat vascular injury models and an in vitro VSMC model. ATF3 was identified as a prominent interacting target of IRF7 that mediates the inhibitory effects of IRF7 on PCNA transcription. Notably, the present findings indicate that IRF7 may represent an attractive therapeutic target for pharmacological or genetic interventions in neointima formation in patients with vascular diseases.

Acknowledgments

We are grateful to Dr Tadatsugu Taniguchi for generously providing IRF7-KO mice.

Sources of Funding

This study was supported by the National Natural Science Foundation of China (nos. 81170086, 81370365, and 81370209), the National Science and Technology Support Project (nos. 2011BAI15B02, 2012BAI39B05, 2013YQ 030923-05, and 2014BAI02B01), the National Basic Research Program of China (no. 2011CB503902), the Ministry of Education New Century Outstanding Talents Support Program (no. NCET-10-0641), the key project of the National Natural Science Foundation (no. 81330005), Natural Science Foundation of Hubei Province of China (grant number 2013CFA077), the Independent Scientific Research Project of Wuhan University (grant number 2042014kf0194).

Disclosures

None.

References

1. Dzau VJ, Braun-Dullaeus RC, Sedding DG. Vascular proliferation and atherosclerosis: new perspectives and therapeutic strategies. *Nat Med*. 2002; 8:1249–1256.
2. Gibbons GH, Dzau VJ. The emerging concept of vascular remodeling. *N Engl J Med*. 1994;330:1431–1438.
3. Er OB, Ma X, Simard T, Pourdjabbar A, Hibbert B. Pathogenesis of neointima formation following vascular injury. *Cardiovasc Hematol Disord Drug Targets*. 2011;11:30–39.
4. Owens GK, Kumar MS, Wamhoff BR. Molecular regulation of vascular smooth muscle cell differentiation in development and disease. *Physiol Rev*. 2004;84:767–801.
5. Indolfi C, Mongiardo A, Curcio A, Torella D. Molecular mechanisms of in-stent restenosis and approach to therapy with eluting stents. *Trends Cardiovasc Med*. 2003;13:142–148.
6. Tamura T, Yanai H, Savitsky D, Taniguchi T. The IRF family transcription factors in immunity and oncogenesis. *Annu Rev Immunol*. 2008;26:535–584.
7. Jiang DS, Wei X, Zhang XF, Liu Y, Zhang Y, Chen K, Gao L, Zhou H, Zhu XH, Liu PP, Bond Lau W, Ma X, Zou Y, Zhang XD, Fan GC, Li H. IRF8 suppresses pathological cardiac remodelling by inhibiting calcineurin signalling. *Nat Commun*. 2014;5:3303.
8. Guo S, Li ZZ, Jiang DS, Lu YY, Liu Y, Gao L, Zhang SM, Lei H, Zhu LH, Zhang XD, Liu DP, Li H. IRF4 is a novel mediator for neuronal survival in ischaemic stroke. *Cell Death Differ*. 2014;21:888–903.
9. Wang XA, Zhang R, She ZG, Zhang XF, Jiang DS, Wang T, Gao L, Deng W, Zhang SM, Zhu LH, Guo S, Chen K, Zhang XD, Liu DP, Li H. Interferon regulatory factor 3 constrains IKKβ/NF-κB signaling to alleviate hepatic steatosis and insulin resistance. *Hepatology*. 2014;59:870–875.

10. Wang XA, Zhang R, Jiang D, Deng W, Zhang S, Deng S, Zhong J, Wang T, Zhu LH, Yang L, Hong S, Guo S, Chen K, Zhang XF, She Z, Chen Y, Yang Q, Zhang XD, Li H. Interferon regulatory factor 9 protects against hepatic insulin resistance and steatosis in male mice. *Hepatology*. 2013;58:603–616.
11. Zhang SM, Gao L, Zhang XF, Zhang R, Zhu LH, Wang PX, Tian S, Yang D, Chen K, Huang L, Zhang XD, Li H. Interferon regulatory factor 8 modulates phenotypic switching of smooth muscle cells by regulating the activity of myocardin. *Mol Cell Biol*. 2014;34:400–414.
12. Honda K, Taniguchi T. IRFs: master regulators of signalling by Toll-like receptors and cytosolic pattern-recognition receptors. *Nat Rev Immunol*. 2006;6:644–658.
13. Hansson GK, Holm J. Interferon-gamma inhibits arterial stenosis after injury. *Circulation*. 1991;84:1266–1272.
14. Palmer H, Libby P. Interferon-beta. A potential autocrine regulator of human vascular smooth muscle cell growth. *Lab Invest*. 1992;66:715–721.
15. Jiang DS, Liu Y, Zhou H, Zhang Y, Zhang XD, Zhang XF, Chen K, Gao L, Peng J, Gong H, Chen Y, Yang Q, Liu PP, Fan GC, Zou Y, Li H. Interferon regulatory factor 7 functions as a novel negative regulator of pathological cardiac hypertrophy. *Hypertension*. 2014;63:713–722.
16. Wang XA, Zhang R, Zhang S, Deng S, Jiang D, Zhong J, Yang L, Wang T, Hong S, Guo S, She ZG, Zhang XD, Li H. Interferon regulatory factor 7 deficiency prevents diet-induced obesity and insulin resistance. *Am J Physiol Endocrinol Metab*. 2013;305:E485–E495.
17. Stevens SL, Leung PY, Vartanian KB, Gopalan B, Yang T, Simon RP, Stenzel-Poore MP. Multiple preconditioning paradigms converge on interferon regulatory factor-dependent signaling to promote tolerance to ischemic brain injury. *J Neurosci*. 2011;31:8456–8463.
18. Leung PY, Stevens SL, Packard AE, Lessov NS, Yang T, Conrad VK, van den Dungen NN, Simon RP, Stenzel-Poore MP. Toll-like receptor 7 preconditioning induces robust neuroprotection against stroke by a novel type I interferon-mediated mechanism. *Stroke*. 2012;43:1383–1389.
19. Buss C, Opitz B, Hocke AC, Lippmann J, van Laak V, Hippenstiel S, Krull M, Suttorp N, Eitel J. Essential role of mitochondrial antiviral signaling, IFN regulatory factor (IRF)3, and IRF7 in chlamydophila pneumoniae-mediated IFN-beta response and control of bacterial replication in human endothelial cells. *J Immunol*. 2010;184:3072–3078.
20. Honda K, Yanai H, Negishi H, Asagiri M, Sato M, Mizutani T, Shimada N, Ohba Y, Takaoka A, Yoshida N, Taniguchi T. IRF-7 is the master regulator of type- I interferon-dependent immune responses. *Nature*. 2005;434:772–777.
21. Hartman MG, Lu D, Kim ML, Kociba GJ, Shukri T, Buteau J, Wang X, Frankel WL, Guttridge D, Prentki M, Grey ST, Ron D, Hai T. Role for activating transcription factor 3 in stress-induced beta-cell apoptosis. *Mol Cell Biol*. 2004;24:5721–5732.
22. Cermak T, Doyle EL, Christian M, Wang L, Zhang Y, Schmidt C, Baller JA, Somia NV, Bogdanove AJ, Voytas DF. Efficient design and assembly of custom TALEN and other TAL effector-based constructs for DNA targeting. *Nucleic Acids Res*. 2011;39:e82.
23. Kuhel DG, Zhu B, Witte DP, Hui DY. Distinction in genetic determinants for injury-induced neointimal hyperplasia and diet-induced atherosclerosis in inbred mice. *Arterioscler Thromb Vasc Biol*. 2002;22:955–960.
24. Sun SG, Zheng B, Han M, Fang XM, Li HX, Miao SB, Su M, Han Y, Shi HJ, Wen JK. miR-146a and Kruppel-like factor 4 form a feedback loop to participate in vascular smooth muscle cell proliferation. *EMBO Rep*. 2011;12:56–62.
25. Li H, He C, Feng J, Zhang Y, Tang Q, Bian Z, Bai X, Zhou H, Jiang H, Heximer SP, Qin M, Huang H, Liu PP, Huang C. Regulator of G protein signaling 5 protects against cardiac hypertrophy and fibrosis during biomechanical stress of pressure overload. *Proc Natl Acad Sci USA*. 2010;107:13818–13823.
26. Blank RS, Owens GK. Platelet-derived growth factor regulates actin isoform expression and growth state in cultured rat aortic smooth muscle cells. *J Cell Physiol*. 1990;142:635–642.
27. Jawien A, Bowen-Pope DF, Lindner V, Schwartz SM, Clowes AW. Platelet-derived growth factor promotes smooth muscle migration and intimal thickening in a rat model of balloon angioplasty. *J Clin Invest*. 1992;89:507–511.
28. Simon DI. Inflammation and vascular injury: basic discovery to drug development. *Circ J*. 2012;76:1811–1818.
29. Azevedo LC, Pedro MA, Souza LC, de Souza HP, Janiszewski M, da Luz PL, Laurindo FR. Oxidative stress as a signaling mechanism of the vascular response to injury: the redox hypothesis of restenosis. *Cardiovasc Res*. 2000;47:436–445.
30. Zhang L, Pagano JS. IRF-7, a new interferon regulatory factor associated with Epstein-Barr virus latency. *Mol Cell Biol*. 1997;17:5748–5757.
31. Au WC, Moore PA, LaFleur DW, Tombal B, Pitha PM. Characterization of the interferon regulatory factor-7 and its potential role in the transcription activation of interferon A genes. *J Biol Chem*. 1998;273:29210–29217.
32. Jin X, Kim SH, Jeon HM, Beck S, Sohn YW, Yin J, Kim JK, Lim YC, Lee JH, Kim SH, Kang SH, Pian X, Song MS, Park JB, Chae YS, Chung YG, Lee SH, Choi YJ, Nam DH, Choi YK, Kim H. Interferon regulatory factor 7 regulates glioma stem cells via interleukin-6 and Notch signalling. *Brain*. 2012;135:1055–1069.
33. Gilliet M, Cao W, Liu YJ. Plasmacytoid dendritic cells: sensing nucleic acids in viral infection and autoimmune diseases. *Nat Rev Immunol*. 2008;8:594–606.
34. Gracias DT, Stelekati E, Hope JL, Boesteanu AC, Doering TA, Norton J, Mueller YM, Fraietta JA, Wherry EJ, Turner M, Katsikis PD. The microRNA miR-155 controls CD8(+) T cell responses by regulating interferon signaling. *Nat Immunol*. 2013;14:593–602.
35. Aly HH, Watashi K, Hijikata M, Kaneko H, Takada Y, Egawa H, Uemoto S, Shimotohno K. Serum-derived hepatitis C virus infectivity in interferon regulatory factor-7-suppressed human primary hepatocytes. *J Hepatol*. 2007;46:26–36.
36. Litvak V, Ratushny AV, Lampano AE, Schmitz F, Huang AC, Raman A, Rust AG, Bergthaler A, Aitchison JD, Aderem A. A FOXO3-IRF7 gene regulatory circuit limits inflammatory sequelae of antiviral responses. *Nature*. 2012;490:421–425.
37. Bidwell BN, Slaney CY, Withana NP, Forster S, Cao Y, Loi S, Andrews D, Mikeska T, Mangan NE, Samarajiwa SA, de Weerd NA, Gould J, Argani P, Moller A, Smyth MJ, Anderson RL, Hertzog PJ, Parker BS. Silencing of Irf7 pathways in breast cancer cells promotes bone metastasis through immune escape. *Nat Med*. 2012;18:1224–1231.
38. Aitman TJ, Critser JK, Cuppen E, Dominiczak A, Fernandez-Suarez XM, Flint J, Gauguier D, Geurts AM, Gould M, Harris PC, Holmdahl R, Hubner N, Izsvak Z, Jacob HJ, Kuramoto T, Kwitek AE, Marrone A, Mashimo T, Moreno C, Mullins J, Mullins L, Olsson T, Pravenec M, Riley L, Saar K, Serikawa T, Shull JD, Szpirer C, Twigger SN, Voigt B, Worley K. Progress and prospects in rat genetics: a community view. *Nat Genet*. 2008;40:516–522.
39. Morita H, Kurihara H, Yoshida S, Saito Y, Shindo T, Oh-Hashi Y, Kurihara Y, Yazaki Y, Nagai R. Diet-induced hyperhomocysteinemia exacerbates neointima formation in rat carotid arteries after balloon injury. *Circulation*. 2001;103:133–139.
40. Meng QH, Yang G, Yang W, Jiang B, Wu L, Wang R. Protective effect of hydrogen sulfide on balloon injury-induced neointima hyperplasia in rat carotid arteries. *Am J Pathol*. 2007;170:1406–1414.
41. Li G, Chen SJ, Oparil S, Chen YF, Thompson JA. Direct in vivo evidence demonstrating neointimal migration of adventitial fibroblasts after balloon injury of rat carotid arteries. *Circulation*. 2000;101:1362–1365.
42. Joung JK, Sander JD. TALENs: a widely applicable technology for targeted genome editing. *Nat Rev Mol Cell Biol*. 2013;14:49–55.
43. Tesson L, Usal C, Menoret S, Leung E, Niles BJ, Remy S, Santiago Y, Vincent AI, Meng X, Zhang L, Gregory PD, Anegon I, Cost GJ. Knockout rats generated by embryo microinjection of TALENs. *Nat Biotechnol*. 2011;29:695–696.
44. Ferguson C, McKay M, Harris RA, Homanics GE. Toll-like receptor 4 (Tlr4) knockout rats produced by transcriptional activator-like effector nuclease (TALEN)-mediated gene inactivation. *Alcohol*. 2013;47:595–599.
45. Suganami T, Yuan X, Shimoda Y, Uchio-Yamada K, Nakagawa N, Shirakawa I, Usami T, Tsukahara T, Nakayama K, Miyamoto Y, Yasuda K, Matsuda J, Kamei Y, Kitajima S, Ogawa Y. Activating transcription factor 3 constitutes a negative feedback mechanism that attenuates saturated Fatty acid/toll-like receptor 4 signaling and macrophage activation in obese adipose tissue. *Circ Res*. 2009;105:25–32.
46. Tamura K, Hua B, Adachi S, Guney I, Kawauchi J, Morioka M, Tamamori-Adachi M, Tanaka Y, Nakabeppu Y, Sunamori M, Sedivy JM, Kitajima S. Stress response gene ATF3 is a target of c-myc in serum-induced cell proliferation. *EMBO J*. 2005;24:2590–2601.
47. Hai T, Wolfgang CD, Marsee DK, Allen AE, Sivaprasad U. ATF3 and stress responses. *Gene Expr*. 1999;7:321–335.
48. Pelzer AE, Bektic J, Haag P, Berger AP, Pycha A, Schafer G, Rogatsch H, Horninger W, Bartsch G, Klocker H. The expression of transcription factor activating transcription factor 3 in the human prostate and its regulation by androgen in prostate cancer. *J Urol*. 2006;175:1517–1522.
49. Janz M, Hummel M, Truss M, Wollert-Wulf B, Mathas S, Johrens K, Hagemeier C, Bommert K, Stein H, Dorken B, Bargou RC. Classical Hodgkin lymphoma is characterized by high constitutive expression of activating transcription factor 3 (ATF3), which promotes viability of Hodgkin/Reed-Sternberg cells. *Blood*. 2006;107:2536–2539.
50. Hagiya K, Yasunaga J, Satou Y, Ohshima K, Matsuoka M. ATF3, an HTLV-1 bZip factor binding protein, promotes proliferation of adult T-cell leukemia cells. *Retrovirology*. 2011;8:19.
51. Allan AL, Albanese C, Pestell RG, LaMarre J. Activating transcription factor 3 induces DNA synthesis and expression of cyclin D1 in hepatocytes. *J Biol Chem*. 2001;276:27272–27280.

52. Cai Q, McReynolds MR, Keck M, Greer KA, Hoying JB, Brooks HL. Vasopressin receptor subtype 2 activation increases cell proliferation in the renal medulla of AQP1 null mice. *Am J Physiol Renal Physiol*. 2007;293: F1858–F1864.

53. Iyer VR, Eisen MB, Ross DT, Schuler G, Moore T, Lee JC, Trent JM, Staudt LM, Hudson J Jr, Boguski MS, Lashkari D, Shalon D, Botstein D, Brown PO. The transcriptional program in the response of human fibroblasts to serum. *Science*. 1999;283:83–87.

54. Xue Y, Lim S, Yang Y, Wang Z, Jensen LD, Hedlund EM, Andersson P, Sasahara M, Larsson O, Galter D, Cao R, Hosaka K, Cao Y. PDGF-BB modulates hematopoiesis and tumor angiogenesis by inducing erythropoietin production in stromal cells. *Nat Med*. 2012;18:100–110.

55. Aung HH, Lame MW, Gohil K, An CI, Wilson DW, Rutledge JC. Induction of ATF3 gene network by triglyceride-rich lipoprotein lipolysis products increases vascular apoptosis and inflammation. *Arterioscler Thromb Vasc Biol*. 2013;33:2088–2096.

56. Lv D, Meng D, Zou FF, Fan L, Zhang P, Yu Y, Fang J. Activating transcription factor 3 regulates survivability and migration of vascular smooth muscle cells. *IUBMB Life*. 2011;63:62–69.

57. Wessely R, Hengst L, Jaschke B, Wegener F, Richter T, Lupetti R, Paschalidis M, Schomig A, Brandl R, Neumann FJ. A central role of interferon regulatory factor-1 for the limitation of neointimal hyperplasia. *Hum Mol Genet*. 2003;12:177–187.

58. Zhang SM, Zhu LH, Li ZZ, Wang PX, Chen HZ, Guan HJ, Jiang DS, Chen K, Zhang XF, Tian S, Yang D, Zhang XD, Li H. Interferon regulatory factor 3 protects against adverse neo-intima formation. *Cardiovasc Res*. 2014;102:469–479.

59. Zhang J, Qian X, Ning H, Yang J, Xiong H, Liu J. Activation of IL-27 p28 gene transcription by interferon regulatory factor 8 in cooperation with interferon regulatory factor 1. *J Biol Chem*. 2010;285:21269–21281.

60. Lindner V, Fingerle J, Reidy MA. Mouse model of arterial injury. *Circ Res*. 1993;73:792–796.